Table 1
Particle characteristics of TiO_2.

	Crystal form	Size
A-1	Anatase	<50 μm
A-2	Anatase	<25 nm
A-3	Anatase	10 nm
R-1	Rutile	<5 μm
R-2	Rutile	30–40 nm
R-3	Rutile	10 nm × 40 nm (spicula)

multimolecular complex termed the inflammasome [14]. The NACHT domain-, leucine-rich repeat-, and pyrin domain (PYD)-containing protein 3 (NALP3) inflammasome, composed of the cytoplasmic receptor NALP3, the adaptor apoptosis-associated speck-like protein containing a CARD domain (ASC), and caspase-1, is implicated in the production of mature IL-1β in response to diverse stimuli [15]. Although the mechanisms of NALP3 activation remain unclear, two separate groups have recently clarified the mediator of NALP3 activation: Cassel et al. demonstrated that phagocytosis of crystalline silica by macrophages induces reactive oxygen species (ROS) production, which contributes to NALP3 activation [16], and Hornung et al. showed that it induces lysosomal destabilization and subsequent release of cathepsin B into the cytoplasm, leading to NALP3 activation [17]. However, it is unclear whether the TiO_2-induced IL-1β production is similarly dependent on NALP3 activation, and it is unknown whether different forms of TiO_2 induce IL-1β production in common or distinct pathways.

Here, we examined the associations between characteristics of forms of TiO_2 and IL-1β production. In addition, we investigated the IL-1β production mechanisms induced by various forms of TiO_2 on macrophage-like THP-1 cells for the creation of novel safe forms of TiO_2.

Materials and methods

Materials and reagents. We used various forms of TiO_2 with two types of crystal structure, different diameters, and different shapes: anatase (A-1 to A-3) and rutile TiO_2 (R-1 to R-3) (Table 1). A-1 to A-3, R-1, and R-2 are spherical, while R-3 is spicular. A-1, A-2, R-1, and R-3 were purchased from Sigma (St. Louis, MO, USA), and A-3 and R-2 were purchased from NanoAmor (Los Alamos, NM, USA). Phorbol 12-myristate 13-acetate (PMA), cytochalasin D, methyl-β-cyclodextrin (MBCD), butylated hydroxyanisole (BHA), diphenyleneiodonium chloride (DPI), and lipopolysaccharide (LPS) were purchased from Sigma. Bafilomycin A_1 was purchased from Biomol (Plymouth Meeting, PA, USA). CA-074-methyl ester (CA-074-Me) and zYVAD-fmk were purchased from Merck Calbiochem (Darmstadt, Germany).

Cells. THP-1 cells (human acute monocytic leukemia cell line) were obtained from the American Type Culture Collection (Manassas, VA, USA) and cultured in RPMI-1640 medium (Wako Pure Chemical Industries, Osaka, Japan) supplemented with 10% fetal bovine serum, 2 mM L-glutamine, and antibiotics at 37 °C in a humid atmosphere with 5% CO_2.

Cytokine production induced by TiO_2. THP-1 cells (1.5×10^4 cells/well) were seeded in 96-well plates (Nunc, Rochester, NY, USA). Differentiation of monocytic THP-1 cells into macrophages was induced by incubation with PMA (0.5 μM) for 24 h at 37 °C. Differentiated cells were then stimulated with 20, 100, or 500 μg/mL TiO_2 for 24 h in the presence or absence of LPS, a widely known activator of THP-1 cells. The levels of IL-1β and tumor necrosis factor α (TNFα) in culture supernatants were then assessed by a commercial enzyme-linked immunosorbent assay (ELISA) kit (BD Pharmingen, San Diego, CA, USA) according to the manufacturer's instructions. For assay of inhibitors, PMA-primed THP-1 cells were washed and pre-incubated with cytochalasin D (1 or 5 μM), MBCD (10 μM), zYVAD-fmk (5 or 10 μM), bafilomycin A_1 (50 or 250 nM), CA-074-Me (5 or 10 μM), BHA (20 or 100 μM), or DPI (10 μM) for 30 min. Then cells were stimulated with 500 μg/mL TiO_2 or 3 mM ATP (a well-known IL-1β inducer) for 6 h in the presence of each inhibitor.

Phagocytosis of TiO_2 on PMA-primed THP-1 cells. THP-1 cells (1.5×10^4 cells/well) were seeded in 96-well plates and primed with PMA (0.5 μM) for 24 h at 37 °C. Differentiated cells were then

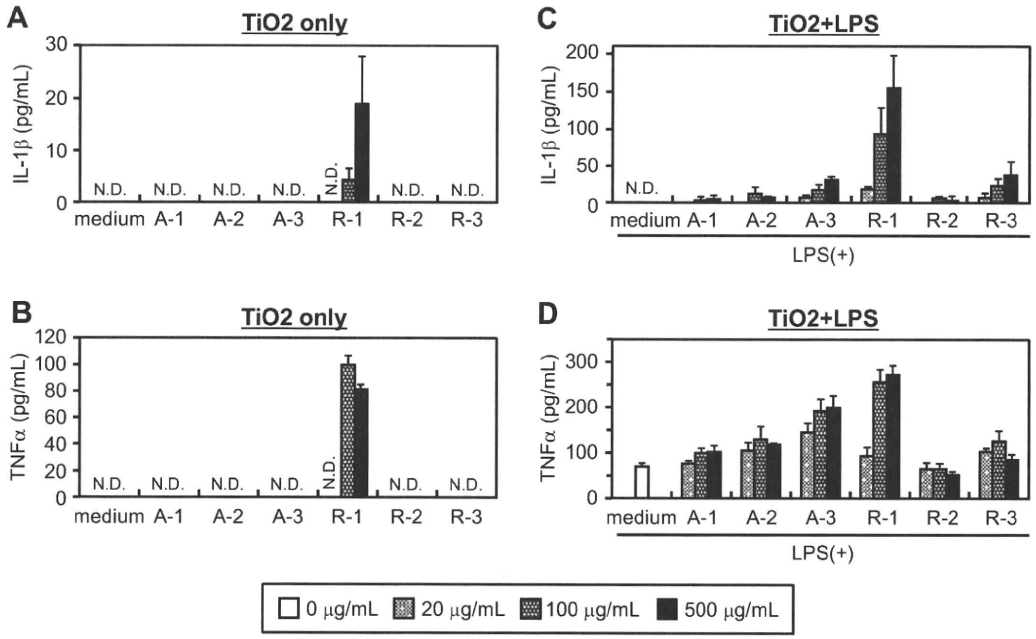

Fig. 1. Association between the characteristics of TiO_2 and cytokine production by THP-1 monocytes. THP-1 monocyte cells were stimulated with 20, 100, or 500 μg/mL of various forms of TiO_2 in the absence (A, B) or presence (C, D) of LPS, and the IL-1β (A, C) or TNFα (B, D) concentrations in the supernatants were evaluated by ELISA. N.D., not detected. Data represent mean ± SD ($n = 4$).

treated with 20 μg/mL TiO_2 for 24 h, and then photographed through a fluorescence microscope (BZ-8000; Keyence Corporation, Osaka, Japan).

Statistical analysis. All results are presented as means ± standard deviation (SD). Differences were compared by Scheffé's method after analysis of variance (ANOVA).

Results and discussion

IL-1β production levels depend on the characteristics of TiO_2

To compare the inflammatory responses, we systematically analyzed the association between characteristics of TiO_2 and levels of IL-1β and TNFα production. We incubated monocytic THP-1 cells with each form of TiO_2 in the absence (Fig. 1A and B) or presence (Fig. 1C and D) of LPS. In the absence of LPS, the larger R-1 induced higher levels of IL-1β and TNFα production than the other forms of TiO_2 (Fig. 1A and B). In the presence of LPS, A-3, and R-3 also induced higher levels of IL-1β production (Fig. 1C). Next we tested PMA-primed macrophage-like THP-1 (THP-1/PMA) cells. Each form of TiO_2 was ingested by THP-1/PMA cells, suggesting that THP-1/PMA cells recognized the TiO_2 as foreign (Fig. 2A). At all concentrations, rutile (especially R-1 and R-3) induced higher IL-1β production than anatase (Fig. 2B). Interestingly, the smallest anatase, A-3, induced higher IL-1β production than the larger A-1 and A-2, whereas the largest rutile, R-1, induced higher IL-1β production than the smaller R-2 and R-3 (Fig. 2B). In addition, spicular R-3 induced higher IL-1β production than the similarly sized and structurally identical but spherical R-2 at the lower concentrations (20 and 100 μg/mL). These results indicate that it is necessary to compare multiple characteristics, including particle size, crystal structure, physical attributes, and surface properties, of TiO_2 to elucidate its biological effects. From these observations, we decided to use A-3, R-1, R-2, and R-3 in further examinations.

Phagocytosis of TiO_2 is an upstream signal in the induction of IL-1β production

Phagocytosis is a key event in initiating macrophage-derived inflammatory responses, and under certain conditions requires lipid raft domains [18,19]. To investigate the association between phagocytosis and TiO_2-induced IL-1β production, we stimulated THP-1/PMA cells with TiO_2 or ATP (control) in the presence of cytochalasin D, a well-characterized inhibitor of phagocytosis that impairs actin-filament assembly. ATP induces IL-1β without cellular internalization and lipid raft formation [20]. Cytochalasin D dramatically abrogated IL-1β production induced by TiO_2, whereas the response to ATP was relatively unaffected (Fig. 3A). Similar results were obtained with MBCD, an inhibitor of lipid raft formation (Fig. 3B). These results indicate that lipid rafts and actin-filament-dependent phagocytosis might be early signals in TiO_2-induced IL-1β production.

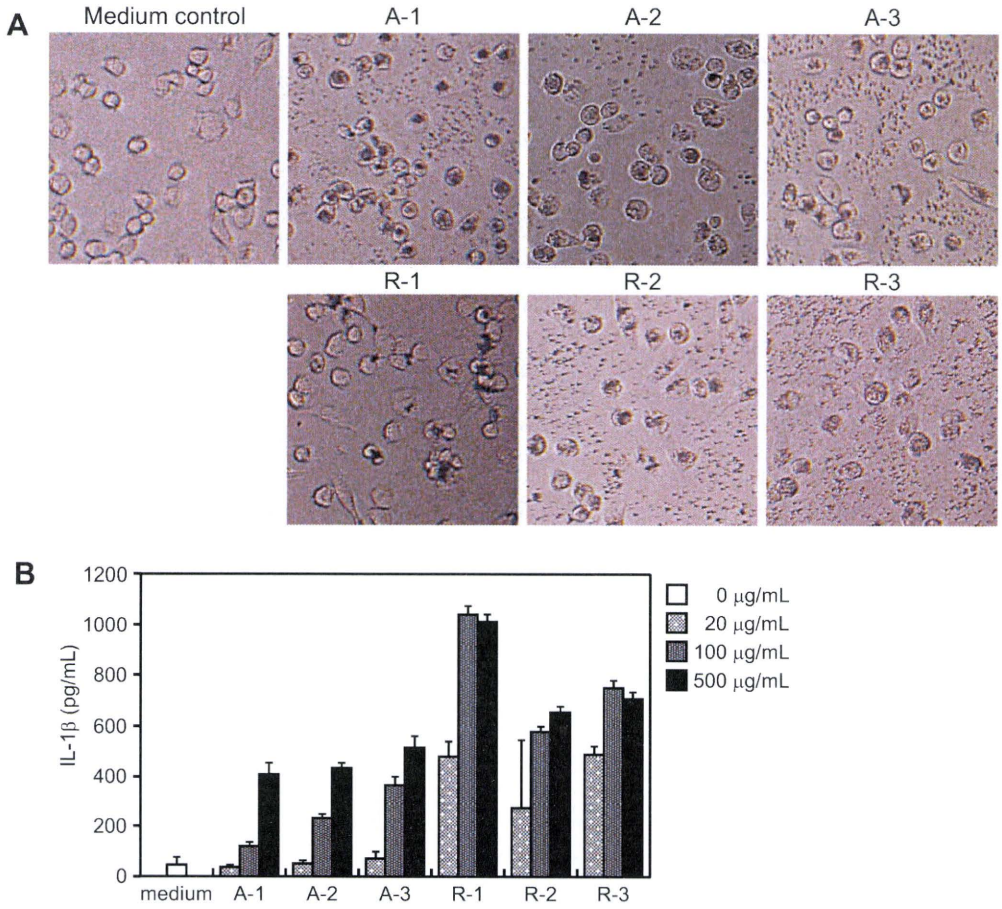

Fig. 2. Association between the characteristics of TiO_2 and cytokine production by differentiated macrophage-like THP-1/PMA cells. (A) THP-1/PMA cells were stimulated with 20 μg/mL of various forms of TiO_2 for 24 h and photographed through a fluorescence microscope. (B) THP-1/PMA cells were stimulated with 20, 100, or 500 μg/mL of various forms of TiO_2 for 6 h, and the IL-1β concentration in the supernatant was evaluated by ELISA. Data represent mean ± SD ($n = 4$; $^{**}P < 0.01$ vs. control).

TiO_2-induced IL-1β production by THP-1/PMA cells depended on caspase-1, ROS, and cathepsin B

Next, we examined how TiO_2 induces IL-1β production. IL-1β is produced from the inactive precursor pro-IL-1β in the cytosol. After cellular activation by a variety of stimuli, the maturation of pro-IL-1β into the mature IL-1β is controlled by caspase-1 [14,21]. To confirm the activation by caspase-1, we treated cells with a caspase-1-specific inhibitor, zYVAD-fmk [22]. zYVAD-fmk completely blocked both ATP- and TiO_2-induced IL-1β production (Fig. 4A), suggesting that the release of IL-1β by TiO_2 is mediated by activated caspase-1.

After assembly of the inflammasome, which activates pro-caspase-1, caspase-1 controls IL-1β maturation. However, how the inflammasome is activated is not well understood. Recently, Hornung et al. reported that crystalline silica induces lysosomal enlargement and loss of lysosomal integrity, leading to the release of the lysosomal contents into the cytoplasm. Furthermore, the release of specific proteases such as cathepsin B seems to be causally related to inflammasome activation [17]. To investigate

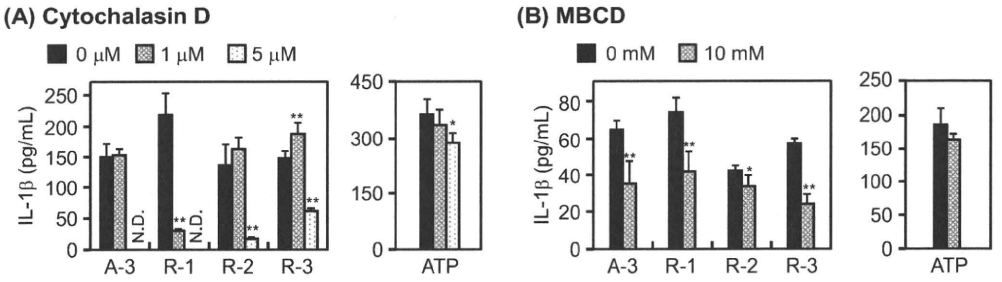

Fig. 3. TiO_2-induced IL-1β production in THP-1/PMA cells is mediated by phagocytosis and lipid rafts. (A, B) IL-1β production levels of THP-1/PMA cells stimulated with 500 μg/mL TiO_2 or 5 mM ATP for 6 h in the presence or absence of (A) cytochalasin D or (B) MBCD at indicated concentrations. IL-1β levels in the culture media were analyzed by ELISA. N.D., not detected. Data represent mean ± SD ($n = 4$; $^{*}P < 0.05$ and $^{**}P < 0.01$ vs. inhibitor [−]).

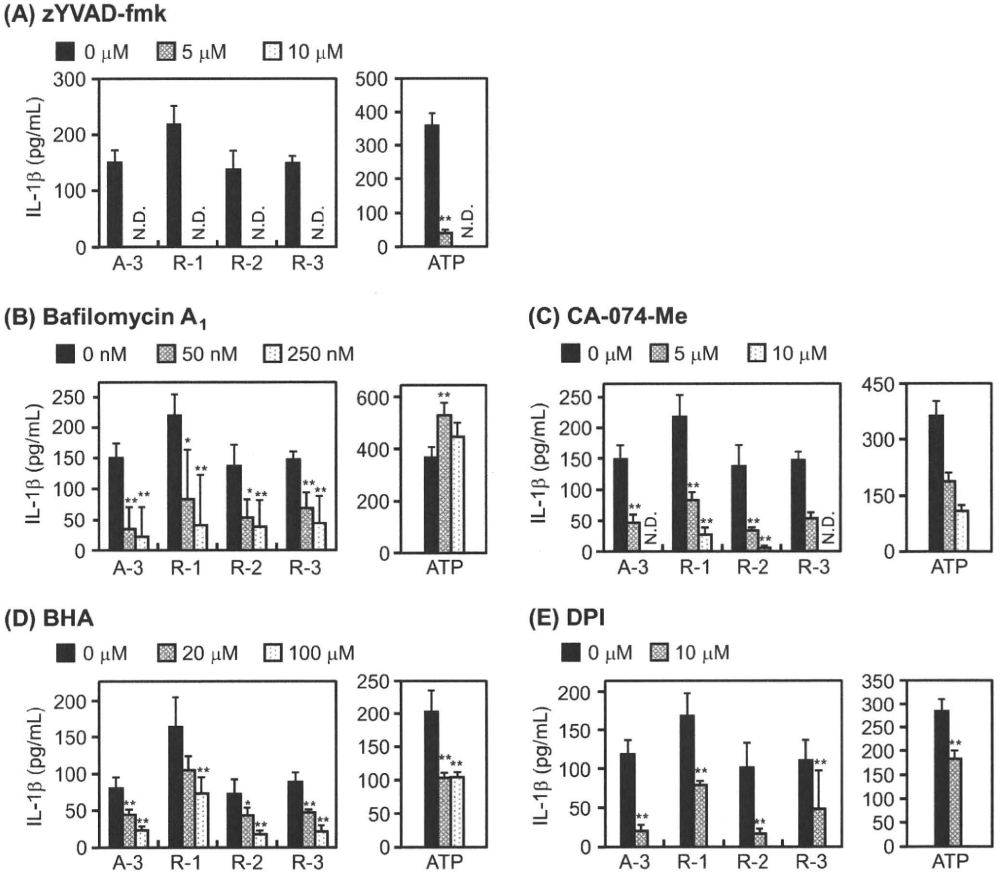

Fig. 4. TiO_2-induced IL-1β production in THP-1/PMA cells is mediated by caspase-1, ROS, and cathepsin B. (A–E) IL-1β production levels of THP-1/PMA cells stimulated with 500 μg/mL TiO_2 or 5 mM ATP for 6 h in the presence or absence of (A) zYVAD-fmk, (B) bafilomycin A_1, (C) CA-074-Me, (D) BHA, or (E) DPI at indicated concentrations. IL-1β levels in the culture media were analyzed by ELISA. N.D., not detected. Data represent mean ± SD ($n = 4$; $^{*}P < 0.05$ and $^{**}P < 0.01$ vs. inhibitor [−]).

whether cathepsin B mediates TiO_2-induced IL-1β production, we stimulated THP-1/PMA cells with TiO_2 in the presence of a specific inhibitor of the vacuolar H^+-ATPase (bafilomycin A_1) or a membrane-permeable cathepsin B-specific inhibitor (CA-074-Me). Bafilomycin A_1 suppresses the pH decrease in endo-lysosomes; the pH decrease is important for cathepsin B to exert its activity. Both inhibitors almost completely suppressed the IL-1β production induced by TiO_2 independent of the characteristics of TiO_2 (Fig. 4B and C), suggesting that the active cathepsin B is one of the most important common activators of the inflammasome upon TiO_2 stimulation.

It is well known that the stimulation of macrophages with TiO_2 induces ROS production. The inflammasome activator ATP can induce the production of ROS, which are important for caspase-1 activation, suggesting that ROS signaling occurs upstream of inflammasome [16,23,24]. To examine whether ROS are involved in the TiO_2-induced IL-1β production, we stimulated THP-1/PMA cells with TiO_2 in the presence of a broad ROS scavenger, BHA. BHA significantly inhibited the TiO_2-induced IL-1β production (Fig. 4D). We obtained similar results in cells treated with DPI, a specific inhibitor of NADPH-oxidase, an important enzyme in the production of ROS (Fig. 4E) [25]. These results indicate that both cathepsin B and ROS play important roles in TiO_2-induced IL-1β production independent of particle characteristics. We speculate that caspase-1, cathepsin B, and ROS are mutually linked in a single pathway for the TiO_2-induced IL-1β-producing cascade. However, it is unclear how the ROS and cathepsin B interact with each other. Recently, Blomgran et al. showed that ROS production in microbes induces lysosomal rupture, allowing cathepsin B to leak into the cytoplasm [26]. Therefore, we speculate that TiO_2-induced ROS induce lysosomal rupture and subsequent inflammasome/caspase-1 activation. On the other hand, some reports show that after phagocytosis of crystalline silica, the reactive particle surface may interact with the phagolysosomal membranes, leading to lysosomal rupture. This suggests that the surface properties of TiO_2 influence the permeability of the lysosomal membrane [27–29]. We are now examining the association between particle characteristics of TiO_2 and lysosomal responses.

Our results confirm that characteristics of TiO_2 change the activity of posttranscriptional processing of IL-1β mediated by caspase-1. However, for several inflammatory cytokines, including IL-1β, both transcription and posttranslational processing are important for the secretion of their mature forms [17,23,30]. Nuclear factor-κB (NFκB) is a well-known transcription factor that regulates the transcription of various cytokines, including IL-1β and TNFα. Therefore, it is important to investigate the association between characteristics of TiO_2 and NFκB activity for the development of safe forms of TiO_2.

The development of safe and effective nanomaterials is important for technology advancement and for healthy lives. For the creation of such materials, we need more information about the relationship between particle characteristics and biological effects. It has become evident that the surface properties of particles are also very important factors in biological effects [7,9,31]. Therefore, we are now trying to develop a novel method for designing TiO_2 particles, including surface properties, crystal structure, size, and shape, to enable the creation of safe and effective novel materials.

Conclusion

The inflammatory effect of TiO_2 depended dramatically on the particle characteristics. TiO_2-induced IL-1β production was mediated by ROS and cathepsin B independent of the particle characteristics. These results provide important basic information for the development of safe forms of TiO_2.

Conflict of interest

The authors declare that they have no conflicts of interest.

Acknowledgments

This study was supported in part by grants from the Ministry of Education, Culture, Sports, Science and Technology of Japan, and the Ministry of Health, Labor and Welfare in Japan.

References

[1] C.L. Tran, D. Buchanan, R.T. Cullen, et al., Inhalation of poorly soluble particles: II. Influence of particle surface area on inflammation and clearance, Inhal. Toxicol. 12 (2000) 1113–1126.
[2] P.M. Hext, J.A. Tomenson, P. Thompson, Titanium dioxide: inhalation toxicology and epidemiology, Ann. Occup. Hyg. 49 (2005) 461–472.
[3] K.E. Driscoll, J.K. Maurer, Cytokine and growth factor release by alveolar macrophages: potential biomarkers of pulmonary toxicity, Toxicol. Pathol. 19 (1991) 398–405.
[4] E. Bermudez, J.B. Mangum, B.A. Wong, et al., Pulmonary responses of mice, rats, and hamsters to subchronic inhalation of ultrafine titanium dioxide particles, Toxicol. Sci. 77 (2004) 347–357.
[5] E.J. Park, J. Yi, K.H. Chung, et al., Oxidative stress and apoptosis induced by titanium dioxide nanoparticles in cultured BEAS-2B cells, Toxicol. Lett. 180 (2008) 222–229.
[6] J. Wang, Y. Liu, F. Jiao, et al., Time-dependent translocation and potential impairment on central nervous system by intranasally instilled TiO(2) nanoparticles, Toxicology 254 (2008) 82–90.
[7] D. Napierska, L.C. Thomassen, V. Rabolli, et al., Size-dependent cytotoxicity of monodisperse silica nanoparticles in human endothelial cells, Small 5 (2009) 846–853.
[8] E.J. Park, J. Yoon, K. Choi, et al., Induction of chronic inflammation in mice treated with titanium dioxide nanoparticles by intratracheal instillation, Toxicology 260 (2009) 37–46.
[9] K.M. Waters, L.M. Masiello, R.C. Zangar, et al., Macrophage responses to silica nanoparticles are highly conserved across particle sizes, Toxicol. Sci. 107 (2009) 553–569.
[10] B.B. Aggarwal, P. Gehlot, Inflammation and cancer: how friendly is the relationship for cancer patients?, Curr Opin. Pharmacol. 9 (2009) 351–369.
[11] L. Franchi, T. Eigenbrod, R. Munoz-Planillo, et al., The inflammasome: a caspase-1-activation platform that regulates immune responses and disease pathogenesis, Nat. Immunol. 10 (2009) 241–247.
[12] P.F. Piguet, C. Vesin, G.E. Grau, et al., Interleukin 1 receptor antagonist (IL-1ra) prevents or cures pulmonary fibrosis elicited in mice by bleomycin or silica, Cytokine 5 (1993) 57–61.
[13] P.N. Hawkins, H.J. Lachmann, M.F. McDermott, Interleukin-1-receptor antagonist in the Muckle–Wells syndrome, N. Engl. J. Med. 348 (2003) 2583–2584.
[14] L. Agostini, F. Martinon, K. Burns, et al., NALP3 forms an IL-1beta-processing inflammasome with increased activity in Muckle–Wells autoinflammatory disorder, Immunity 20 (2004) 319–325.
[15] A. Halle, V. Hornung, G.C. Petzold, et al., The NALP3 inflammasome is involved in the innate immune response to amyloid-beta, Nat. Immunol. 9 (2008) 857–865.
[16] S.L. Cassel, S.C. Eisenbarth, S.S. Iyer, et al., The Nalp3 inflammasome is essential for the development of silicosis, Proc. Natl. Acad. Sci. USA 105 (2008) 9035–9040.
[17] V. Hornung, F. Bauernfeind, A. Halle, et al., Silica crystals and aluminum salts activate the NALP3 inflammasome through phagosomal destabilization, Nat. Immunol. 9 (2008) 847–856.
[18] M. Kirkham, R.G. Parton, Clathrin-independent endocytosis: new insights into caveolae and non-caveolar lipid raft carriers, Biochim. Biophys. Acta 1745 (2005) 273–286.
[19] M.F. Hanzal-Bayer, J.F. Hancock, Lipid rafts and membrane traffic, FEBS Lett. 581 (2007) 2098–2104.
[20] C.M. Cruz, A. Rinna, H.J. Forman, et al., ATP activates a reactive oxygen species-dependent oxidative stress response and secretion of proinflammatory cytokines in macrophages, J. Biol. Chem. 282 (2007) 2871–2879.
[21] F. Martinon, V. Petrilli, A. Mayor, et al., Gout-associated uric acid crystals activate the NALP3 inflammasome, Nature 440 (2006) 237–241.
[22] S. Mariathasan, D.S. Weiss, K. Newton, et al., Cryopyrin activates the inflammasome in response to toxins and ATP, Nature 440 (2006) 228–232.
[23] C. Dostert, V. Petrilli, R. Van Bruggen, et al., Innate immune activation through Nalp3 inflammasome sensing of asbestos and silica, Science 320 (2008) 674–677.
[24] M.E. Carlotti, E. Ugazio, S. Sapino, et al., Role of particle coating in controlling skin damage photoinduced by titania nanoparticles, Free Radic. Res. 43 (2009) 312–322.
[25] F. Morel, J. Doussiere, P.V. Vignais, The superoxide-generating oxidase of phagocytic cells. Physiological, molecular and pathological aspects, Eur. J. Biochem. 201 (1991) 523–546.

[26] R. Blomgran, L. Zheng, O. Stendahl, Cathepsin-cleaved Bid promotes apoptosis in human neutrophils via oxidative stress-induced lysosomal membrane permeabilization, J. Leukoc. Biol. 81 (2007) 1213–1223.
[27] A.C. Allison, J.S. Harington, M. Birbeck, An examination of the cytotoxic effects of silica on macrophages, J. Exp. Med. 124 (1966) 141–154.
[28] S. Nadler, S. Goldfischer, The intracellular release of lysosomal contents in macrophages that have ingested silica, J. Histochem. Cytochem. 18 (1970) 368–371.
[29] G. Erdogdu, V. Hasirci, An overview of the role of mineral solubility in silicosis and asbestosis, Environ. Res. 78 (1998) 38–42.
[30] S.D. Ha, A. Martins, K. Khazaie, et al., Cathepsin B is involved in the trafficking of TNF-alpha-containing vesicles to the plasma membrane in macrophages, J. Immunol. 181 (2008) 690–697.
[31] X. He, H. Nie, K. Wang, et al., In vivo study of biodistribution and urinary excretion of surface-modified silica nanoparticles, Anal. Chem. 80 (2008) 9597–9603.

Graduate School of Pharmaceutical Sciences[1], Osaka University; Laboratory of Pharmaceutical Proteomics[2], National Institute of Biomedical Innovation; The Center for Advanced Medical Engineering and Informatics[3], Osaka University; Bioresources Research[4], Laboratory of Common Apparatus, National Institute of Biomedical Innovation, Osaka, Japan

Size-dependent cytotoxic effects of amorphous silica nanoparticles on Langerhans cells

H. NABESHI[1,2,*], T. YOSHIKAWA[1,2,*], K. MATSUYAMA[1,2], Y. NAKAZATO[1,2], A. ARIMORI[1,2], M. ISOBE[1,2], S. TOCHIGI[1,2], S. KONDOH[1,2], T. HIRAI[1,2], T. AKASE[1,2], T. YAMASHITA[1,2], K. YAMASHITA[1,2], T. YOSHIDA[1,2], K. NAGANO[2], Y. ABE[2], Y. YOSHIOKA[2,3], H. KAMADA[2,3], T. IMAZAWA[4], N. ITOH[1], S. TSUNODA[1,2,3,**], Y. TSUTSUMI[1,2,3]

Received August 10, 2009, accepted August 14, 2009

Tomoaki Yoshikawa, Ph.D. and Yasuo Tsutsumi, Ph.D., Department of Toxicology, Graduate School of Pharmaceutical Sciences, Osaka University, 1-6 Yamadaoka, Suita, Osaka 565-0871, Japan
tomoaki@phs.osaka-u.ac.jp
**These authors contributed equally to the work.*
***Shin-ichi Tsunoda, Ph.D., Laboratory of Pharmaceutical Proteomics, National Institute of Biomedical Innovation, 7-6-8 Saito-Asagi, Ibaraki, Osaka 567-0085, Japan.*

Pharmazie 65: 199–201 (2010) *doi: 10.1691/ph.2010.9268*

Amorphous silica nanoparticles (nSPs), are widely used in medicines, cosmetics and food. However, due to their reduced particle size they are suspected to pose new risks induced by changes in biological reactivity and kinetics, which differ from those of bulk materials. In a previous study, we showed that silica particles with a diameter of 70 nm penetrated the stratum corneum (SC) of mouse skin and were taken up by living cells such as keratinocytes and Langerhans cells. To clarify the relationship between particle size, distribution and cellular response, we have evaluated size-dependent intracellular localization and cytotoxicity of silica particles, using the mouse epidermal Langerhans cell line XS52. On treatment with silica particles of diameters 70, 300, and 1000 nm, cellular uptake and cytotoxicity increased with reduction in particle size. These results suggest that smaller sized silica particles induced greater cytotoxicity against Langerhans cells, which was correlated with the quantity of particle uptake into the cells.

1. Introduction

The recent development of nanoscale engineering represents a current dynamic area of interdisciplinary research, incorporating nanomaterials (NMs) into a diverse product matrix such as diagnostics, food additives and cosmetics. Because amorphous silica nanoparticles (nSPs) and titanium oxide nanoparticles, etc. are colorless and reflect ultraviolet more efficiently than micro-sized particles, nSPs and titanium oxide nanoparticles are already used as cosmetic vehicles or functional ingredients in many cosmetics such as foundation creams and sunscreens. However, because NMs may possess novel properties, kinetics, and biological effects different from those of micro size bulk materials, their potential harmful effects on humans are raising concerns about their safety. Thus, there is an urgent need for risk assessment of NMs. To achieve this, it is most important to analyze the relationship between particle-size parameters, cellular distribution and biological effects, allowing prediction and avoidance of risk in using NMs.

In a previous study, we showed that silica particles with a diameter of 70 nm penetrated the stratum corneum (SC) of mouse skin and were taken up by living cells such as keratinocytes and Langerhans cells. So, to reveal the relationship between particle size, distribution, and cellular response, we evaluated size-dependent intracellular localization and cytotoxicity of silica particles, using the mouse epidermal Langerhans cell line XS52.

2. Investigations, results and discussion

To assess cellular uptake of nSPs, we observed XS52 cells treated with 100 μg/ml nSP70, nSP300 and mSP1000 using transmission electron microscopy (TEM). We found that nSP300 and mSP1000 were located in cytoplasm only (Fig. 1c and d), while nSP70 was surprisingly located in nucleus as well as cytoplasm (Fig.1a and b). Furthermore the quantity of silica particles taken up by the cells increased as particle size decreased. These results suggested that the uptake and localization of silica particles altered with particle size.

We next investigated biological effects of various-sized silica particles in XS52 cells. To assess the effect of treatments with nSPs on cellular proliferation, the [^{3}H]-thymidine incorporation assay was performed. As shown in Fig. 2, XS52 cell proliferation was dose-dependently inhibited by treatment with silica particles of all sizes. IC50 values for nSP70, nSP300 and mSP1000 were 4.2, 32.6, and 75.0 μg/ml, respectively. These results showed that the growth of XS52 cells was more strongly inhibited by smaller-sized nSP.

To study the mechanism responsible for the effects on XS52 cells treated with various-sized silica particles, we measured the quantity of lactate dehydrogenase (LDH) released. LDH is released into culture medium after the cellular membrane disruption that constitutes the last step of the in vitro cell death process. After 24 h of exposure (Fig. 3), no LDH release was observed in mSP1000-treated cells, while dose-dependent LDH

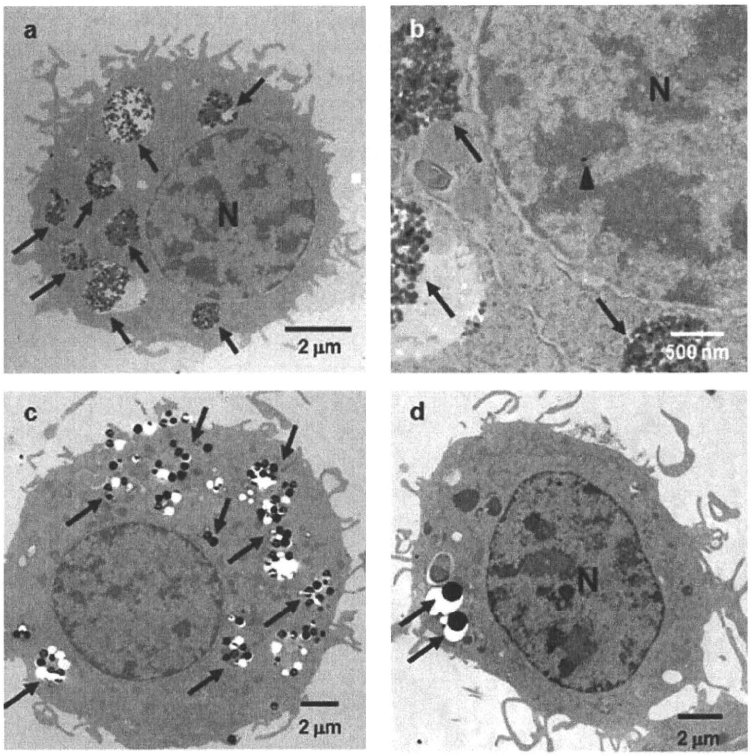

Fig. 1: Localization of silica particles in XS52 cells (arrows). Cells were treated for 24 h with nSP70 (a and b), nSP300 (c) and mSP1000 (d). nSP300 and mSP1000 were located in cytoplasm only. On the other hand, nSP70 was located in the nucleus as well as in cytoplasm (b, arrow head). Scale bars; 2 µm (a, c and d), 500 nm (b)

release was observed in nSP70- and nSP300-treated cells. The highest LDH release was recorded on treatment with 30 µg/ml nSP70 (193 ± 6.8% of control). This result therefore indicated that the cytotoxicity to XS52 cells may be due to cellular membrane damage. Consequently, it appears that the difference in the quantity of silica particles taken up by the cells may explain the size-dependent toxicity to XS52 cells.

As reported elsewhere, we had shown that nSP70 penetrated the stratum corneum (SC) of mouse skin and was taken up by living Langerhans cells (Nabeshi et al. 2010). Furthermore, in the present study we showed that the difference in the quantity of silica particles taken up by the cells was linked to size-dependent toxicity and nSP70 taken up by Langerhans cells entered the nucleus. Thus, our previous and present results suggest that transdermal exposure to nSPs may (i) risk dysfunction of Langerhans cells, as shown by the cytotoxicity to XS52 cells, (ii) induce immune disruption by altering the immune response (Tinkle et al. 2003; Fifis et al. 2004) and (iii) induce dysfunction of the nucleus and genotoxicity via aggregation of intranuclear protein or inhibition of RNA transcription (Chen and von Mikecz 2005) following entrance of nSPs into the nucleus.

Collectively, the data obtained in this study offer highly useful information for prediction and avoidance of harmful effects mediated by nSPs used commercially in cosmetics. Thus, cor-

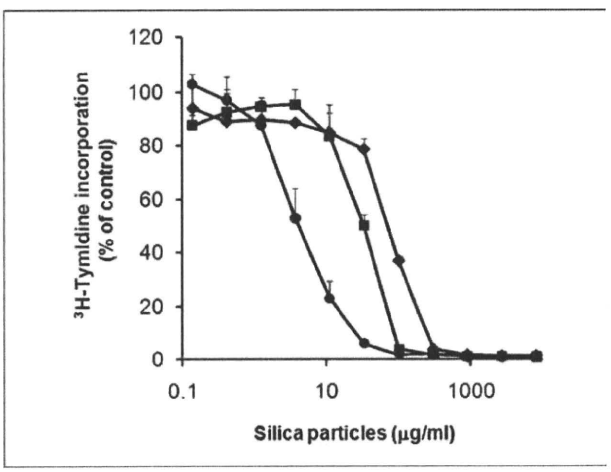

Fig. 2: Effect of various-sized silica particles on proliferation of XS52 cells. The proliferation of cells after incubation with nSP70 (circle), nSP300 (square) and mSP1000 (diamond) for 24 h was evaluated using the [^{3}H]-thymidine incorporation assay. The percentage increase in cell proliferation was calculated relative to the negative control. Data are presented as means ± SD

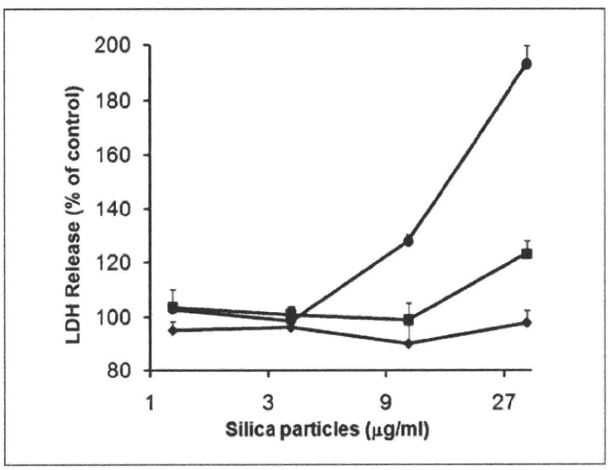

Fig. 3: Effect of silica particles on membrane damage. Cellular membrane damage in XS52 cells after incubation with nSP70 (circle), nSP300 (square) and mSP1000 (diamond) for 24 h was evaluated by the LDH release assay. The percentage cellular membrane damage was calculated relative to the negative (medium) controls. Data are presented as means ± SD

related analysis of physicochemical properties, harmful effects and biodistribution as performed in our study may offer valuable readouts for toxicity of nanomaterials and help to develop non-toxic nanomaterials in the future.

3. Experimental

3.1. Silica particles

Fluorescent (red-F)-labeled silica particle suspensions (25 mg/ml or 50 mg/ml) with a diameter of 70, 300 and 1000 nm (Micromod Partikeltechnologie GmbH, Rostock, Germany; designated nSP70, nSP300, mSP1000, respectively) were used in this study. In each case, silica particles were used after 5 min sonication and 1 min vortexing.

3.2. Cell culture

Cells from the Langerhans cell-like line XS52 (a kind gift of Akira Takashima, University of Toledo, Health Science Campus, Toledo) were expanded in complete medium containing 2 ng/ml murine GM-CSF and 10% culture supernatants from skin-derived stromal NS47 cells (a kind gift of Akira Takashima). Complete medium was RPMI-1640 medium supplemented with 10% heat- inactivated fetal calf serum, 1% non-essential amino acids, 1% L-glutamine, 1 mM sodium pyruvate, 1% 2-mercaptoethanol, 10 mM HEPES buffer, and 1% Antibiotic-Antimycotic Mix stock solution.

3.3. Transmission electron microscopy (TEM) analysis of Langerhans cell line

XS52 cells were cultured with various-sized silica particles for 24 h on chamber slides, then fixed at 4 °C in 2.5% glutaraldehyde and washed three times in 0.1 M phosphate buffer (pH: 7.4); cells were then post-fixed in phosphate-buffered 1% osmium tetroxide for 60 min at 4 °C, dehydrated through a series of ethanol concentrations and embedded in EPON resin (TAAB, Watford, UK). Ultrathin sections were stained with lead citrate and examined under an electron microscope (Hitachi H-7650).

3.4. [^{3}H]-Thymidine incorporation assay

Proliferation of silica particle-treated XS52 cells was measured by [^{3}H]-thymidine incorporation assay. 1×10^4 cells were cultured with varying concentrations of nSPs for 18 h at 37 °C and [^{3}H] thymidine (1 μCi/well) was then added into each well. After a further 6 h, cells were harvested and lysed on glass fiber filter plates using a Cell harvester (PerkinElmer, MA, USA). The filter plates were then dried and counted by standard liquid scintillation counting techniques in a TopCounter (PerkinElmer, MA, USA).

3.5. LDH release assay

Lactate dehydrogenase (LDH) activity of XS52 cells exposed to nSP70, nSP300, mSP1000 was determined using a commercial LDH cytotoxicity test (WAKO, Osaka, Japan) according to the manufacturer's instructions. In brief, 5×10^3 cells were seeded into each well of a 96 well plate. After 24 h incubation, cells were treated with nSP70, nSP300, mSP1000 or 0.2% Tween 20 (positive control). After a further 24 h incubation period, 50 μl of medium overlying cells was used for LDH analysis. Absorption of light at 560 nm was measured using a spectrophotometer.

Acknowledgement: This study was supported in part by Grants-in-Aid for Scientific Research from the Ministry of Education, Culture, Sports, Science and Technology of Japan, and in part by Grants-in-Aid for Scientific Research from the Japanese Society for the Promotion of Science (JSPS). The study was also supported in part by Health Labour Sciences Research Grants from the Ministry of Health, Labor and Welfare of Japan, in part by Health Sciences Research Grants for Research on Publicly Essential Drugs and Medical Devices from the Japan Health Sciences Foundation, in part by a Grant from the Ministry of the Environment, and in part by the Nagai Foundation Tokyo.

References

Bennett CL, van Rijn E, Jung S, Inaba K, Steinman RM, Kapsenberg ML, Clausen BE (2005) Inducible ablation of mouse Langerhans cells diminishes but fails to abrogate contact hypersensitivity. J Cell Biol 169: 569–576.

Chen M, von Mikecz A (2005) Formation of nucleoplasmic protein aggregates impairs nuclear function in response to SiO2 nanoparticles. Exp Cell Res 305: 51–62.

Fifis T, Gamvrellis A, Crimeen-Irwin B, Pietersz GA, Li J, Mottram PL, McKenzie IF, Plebanski M (2004) Size-dependent immunogenicity: therapeutic and protective properties of nano-vaccines against tumors. J Immunol 173: 3148–3154.

Nabeshi H, Yoshikawa T, Matsuyama K, Nakazato Y, Matsuo K, Arimori A, Isobe M, Tochigi S, Kondoh S, Hirai T, Akase T, Yamashita T, Nagano K, Abe Y, Yoshioka Y, Kamada H, Imazawa T, Nakagawa S, Mayumi T, Itoh N, Tsunoda S, Tsutsumi Y (2010) NanoTox studies of nanosilica for ensuring safety-2. In preparation.

Palucka K, Banchereau J (2002) How dendritic cells and microbes interact to elicit or subvert protective immune responses. Curr Opin Immunol 14: 420–431.

Tinkle SS, Antonini JM, Rich BA, Roberts JR, Salmen R, DePree K, Adkins EJ (2003) Skin as a route of exposure and sensitization in chronic beryllium disease. Environ Health Perspect 111: 1202–1208.

Inflammation, Vol. 33, No. 4, August 2010 (© 2010)
DOI: 10.1007/s10753-010-9182-7

Carbon Nanotubes Elicit DNA Damage and Inflammatory Response Relative to Their Size and Shape

Kohei Yamashita,[1,2] Yasuo Yoshioka,[1,2,3,5] Kazuma Higashisaka,[1,2] Yuki Morishita,[1,2] Tokuyuki Yoshida,[1,2] Maho Fujimura,[1,2] Hiroyuki Kayamuro,[1,2] Hiromi Nabeshi,[1,2] Takuya Yamashita,[1,2] Kazuya Nagano,[2] Yasuhiro Abe,[2] Haruhiko Kamada,[2,3] Yuichi Kawai,[4] Tadanori Mayumi,[4] Tomoaki Yoshikawa,[1,2] Norio Itoh,[1] Shin-ichi Tsunoda,[1,2,3,5] and Yasuo Tsutsumi[1,2,3,5]

Abstract—Carbon nanotubes (CNTs) have been one of the most extensively researched and developed nanomaterials. However, little concern has been placed on their safety. The biological effects of CNTs are believed to differ relative to size and shape. Thus, the relationship between the characteristics of CNTs and their safety needs to be evaluated. In this study, we examined the biological effects of different-sized multi-walled CNTs (MWCNTs) and single-walled CNTs (SWCNTs). Long and thick MWCNTs induced the strongest DNA damage while similar SWCNTs caused little effect. Comparison of inflammatory responses of various types of CNTs found that peritoneal CNT administration of long and thick MWCNTs increased the total cell number in abdominal lavage fluid in mice. These results indicate that long and thick MWCNT, but not short and thin MWCNT, cause DNA damage and severe inflammatory effects. These findings might provide useful information for constructing novel CNTs with safety.

KEY WORDS: carbon nanotubes; cytotoxicity; DNA damage; inflammation; nanomaterial.

INTRODUCTION

Nanomaterials are typically defined as engineered structures having at least one dimension of ≤100 nm [1]. Particles of this size have a high surface area and can be modified for preparation of materials with unique physicochemical properties, such as high conductivity, strength, durability, and chemical reactivity [2]. A diverse array of nanomaterials such as nanosilicas, fullerenes, and carbon nanotubes (CNTs) has been prepared. Such nanomaterials are already being used in electronics, sunscreens, cosmetics, diagnostic medicines, and imaging and drug-delivery systems worldwide [2, 3].

CNTs have been one of the most extensively researched and developed nanomaterials [3]. CNTs are unique cylinder structures with a diameter of a few nanometers and length ranging from nano- to micrometers [4]. There are two types of CNTs, single-walled CNTs (SWCNTs) comprised of one cylinder and multi-walled (MWCNTs) comprised of two to 50 cylinders concentrically stacked with a common long axis. The use of CNTs in industrial devices is increasing for applications in manufactured and medical products [2, 3, 5]. The global market for CNTs is predicted to grow to US $2 billion and a ton of CNTs are being produced worldwide every year.

Kohei Yamashita and Yasuo Yoshioka contributed equally to this work.

[1] Department of Toxicology, Graduate School of Pharmaceutical Sciences, Osaka University, 1-6, Yamadaoka, Suita, Osaka 565-0871, Japan
[2] Laboratory of Pharmaceutical Proteomics, National Institute of Biomedical Innovation (NiBio), 7-6-8 Saito-asagi, Ibaraki, Osaka 567-0085, Japan
[3] The Center for Advanced Medical Engineering and Informatics, Osaka University, 1-6, Yamadaoka, Suita, Osaka 565-0871, Japan
[4] Graduate School of Pharmaceutical Sciences, Kobegakuin University, 1-1-3, Minatojima, Chuo-ku, Kobe, 650-8586, Japan
[5] To whom correspondence should be addressed at Department of Toxicology, Graduate School of Pharmaceutical Sciences, Osaka University, 1-6, Yamadaoka, Suita, Osaka 565-0871, Japan; and National Institute of Biomedical Innovation (NiBio), 7-6-8 Saito-asagi, Ibaraki, Osaka 567-0085, Japan. E-mail: yasuo@phs.osaka-u.ac.jp; tsunoda@nibio.go.jp; ytsutsumi@phs.osaka-u.ac.jp

With the increased use of CNTs, public concern about their potential risks to human health has also risen [6, 7]. In fact, CNTs have been the focus of much research as it may be a likely driver of adverse health effects, such as exacerbation of airway diseases [7]. In addition, MWCNTs have been reported to induce mesothelioma-like lesions in mice and rats upon injection, in a similar manner to crocidolite asbestos [8–10]. Therefore, there are concerns that these nano-scale, needle-like CNTs may also contribute to such toxicity as seen for asbestos and other pathogenic fibers. While a number of problems of CNTs have been reported, little information is known regarding the relationship to their molecular size/shape and toxicity. Therefore, the safety of CNTs relative to their size and shape requires investigation. In this study, we analyzed the relationship between the characteristics of CNTs and toxicity including DNA damage and the inflammatory effect.

MATERIALS AND METHODS

CNTs. Three different MWCNTs (M1, M2, and M3) and one SWCNT (S4) were purchased from SES research (Houston, TX, USA) and Meijo Nano Carbon Co. Ltd (Aichi, Japan). These CNTs were prepared for experimental use by 30 min ultrasonication in a 0.001% Triton X-100 (Sigma-Aldrich, Tokyo, Japan)/MilliQ water solution. The characteristics of CNTs supplied by the manufacturers are as follows: M1 (Meijo Nano Carbon), length 5–15 μm, diameter 20–60 nm; M2 (SES research), length 1–2 μm, diameter 60–100 nm; M3 (SES research), length 1–2 μm, diameter <10 nm; and S4 (SES research), length 5–15 μm, diameter <2 nm.

Cell Culture and Mice. A549 cells (human alveolar carcinoma epithelial cells) and THP-1 cells (human monocytic cells) were purchased from American Type Culture Collection (Manassas, VA, USA). A549 cells were cultured in Dulbecco's modified Eagle's medium (Wako Pure Chemical Industries, Osaka, Japan) supplemented with 10% fetal bovine serum (FBS), 2 mM L-glutamine, 100μg/ml penicillin, and 100 U/ml streptomycin. THP-1 cells were cultured in RPMI 1640 (Wako Pure Chemical Industries) supplemented with 10% FBS, 2 mM L-glutamine, 0.05 mM 2-mercaptoethanol, 100 μg/ml penicillin, and 100 U/ml streptomycin. Female C57BL/6 mice were purchased from Nippon SLC (Shizuoka, Japan) and used at 6 to 8 weeks of age. All of the animal experimental procedures were performed in accordance with the institutional ethical guidelines for the animal experiments.

Cytotoxic Assay. A549 cells were seeded at 1×10^4/well in 96-well plates and incubated for 24 h at 37°C. Cells were cultured in a serial dilution of CNTs. After 24 h incubation, cell survival was determined using the methylene blue assay as described previously [11]. Briefly, the cells were fixed using glutaraldehyde and stained with 0.05% methylene blue for 15 min. After washing with phosphate-buffered saline, 0.33 N HCl was added to each well and the absorbance of the released dye was measured at 655/415 nm.

Comet Assay. Detection of DNA strand breaks and alkaline labile sites in A549 cells was examined by single cell gel electrophoresis (comet assay) after CNT exposure. A549 cells were cultured in six-well plates (Nunc, Roskilde, Denmark) 24 h prior to exposure. Semiconfluent cultures were exposed for 3 h with 50μg/ml CNTs. The comet assay was performed by Comet Assay Kit (Trevigen, Gaitherburg, MD, USA) according to the manufacturer's instructions. The slides were coded, and one scorer performed the comet analysis using a fluorescence microscope (Olympus, Tokyo, Japan). At least 90 cells per sample (three replicates, each with 30 cells/slide) were analyzed using the comet image analysis software (Youworks, Tokyo, Japan), and the percentage of DNA, tail length, and tail moment in the comet tail were used as a measure of the amount of DNA damage. As a positive control, we used A549 cells exposed to hydrogen peroxide and untreated A549 cells as a negative control.

Inflammatory Responses In Vivo. C57BL/6 mice were intraperitoneally injected with each CNT dissolved in a 0.001% TritonX-100/MilliQ water solution, allowing for an overall exposure of 50μg per mice. After 24 h treatment, abdominal cavity lavage fluid was recovered with two 2-ml washes of ice-cold sterile saline. The lavage fluid was centrifuged at 123×*g* for 5 min at 4°C and the cell pellets were resuspended in 0.5 ml saline solution. The total cell number was determined using NucleoCounter (Chemometec, Osaka, Japan).

Statistical Analysis. All results are presented as means±standard deviation (SD) or standard error of the mean (SEM). Statistical significance in differences was evaluated by Bonferroni's method after analysis of variance (ANOVA).

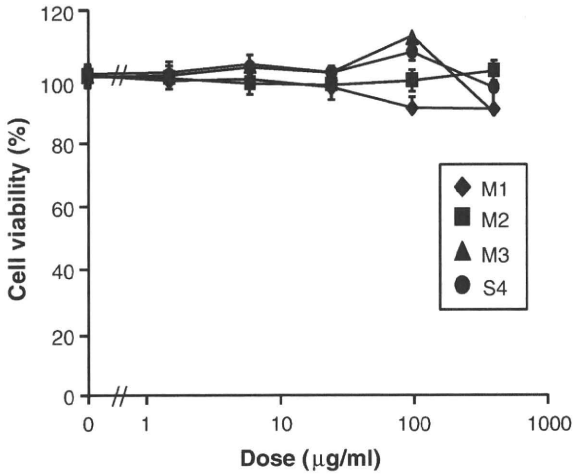

Fig. 1. Cell viability of A549 cells treated with CNTs of different size and shape. Cytotoxicity was measured after 24 h exposure to CNTs using methylene blue assay. Data represent means±SD.

RESULTS AND DISCUSSION

Recently, CNTs have been considered useful as devices for medical and industrial markets. However, concerns of their toxicity and carcinogenicity have increased as they have comparable structures to asbestos. In this study, we evaluated the relationship between the toxicity of CNTs and their characteristic length and width.

We used three different MWCNTs (M1, M2, and M3) and SWCNT (S4). The characteristics of CNTs are described in "Materials and Methods". First, we examined the cytotoxicity of CNTs by a methylene blue assay using A549 human lung cells (Fig. 1). We found no cytotoxicity of any CNT on A549 cells at the range of doses examined. To evaluate the effect of CNT exposure on DNA damage, we then detected DNA fragmentation by the comet assay, which is an uncomplicated and sensitive technique for the detection of DNA damage at the level of the individual eukaryotic cell. After 3 h incubation in the absence or presence of different kinds

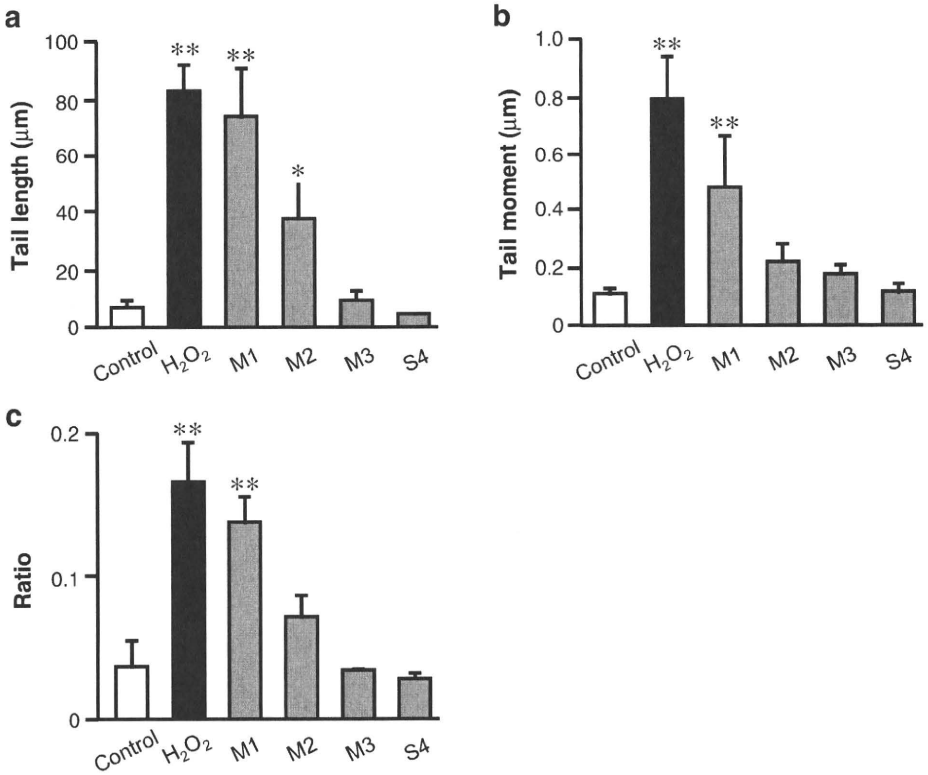

Fig. 2. DNA damage in cultured A549 cells treated with CNTs of different size and shape. DNA damage in cultured A549 cells was examined after 3 h exposure to 50μg/ml CNTs. **a** The damage is measured as DNA in tail, **b** DNA in tail moment, and **c** the ratio of the tail length to head diameter by the Comet assay. Hydrogen peroxide (0.5 mM) was used as the positive control. Data represent means±SD (*$P<0.05$, **$P<0.01$ compared with control group by ANOVA).

of CNTs, A549 cells were subjected to the comet assay (Fig. 2). Significant DNA damage was observed in M1, which is the longest and thickest MWCNT. While M2 caused some DNA damage, M3 and S4 hardly caused any DNA damage. The length of S4 is almost the same as M1, suggesting that DNA damage is not entirely dependent on length, but also on the shape of CNTs. These results also indicate that the combined parameters of thickness and length affect DNA damage relative to size and shape. As reactive oxygen species are known to cause DNA damage [12], whereby insufficient cellular repair mechanisms induce additional changes in DNA of tumor cells to make those cells malignant, their relationship to the size/shape of CNTs should also be examined.

Inflammation is a hallmark of exposure to asbestos or CNTs. This response has been observed both in CNT- and asbestos-treated animal models as well as in patients with asbestos-related lung disease [7, 13, 14]. Inflammation is believed to increase the risk of cancer progression [15, 16]. In fact, inflammatory cytokines are implicated in the pathogenesis of asbestosis and mesothelioma [17, 18]. Thus, we compared the inflammatory responses of CNTs *in vivo*. Each CNT (50 μg) was intraperitoneally injected in C57BL/6 mice and the number of infiltrating inflammatory cells into the peritoneal cavity was measured after 24 h

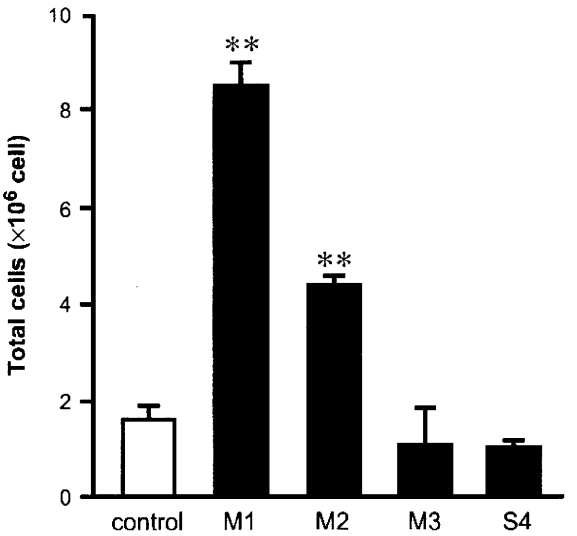

Fig. 3. Inflammatory response induced by CNTs of different size and shape *in vivo*. C57BL/6 mice were intraperitoneally injected with 50 μg CNTs (*M1*, *M2*, *M3*, and *S4*). After 24-h post-exposure, the abdominal lavage fluid was harvested and the total cell number was determined to evaluate inflammatory responses induced by CNTs. Data represent means±SEM (n=5, $^{**}P<0.01$ compared with control group by ANOVA).

(Fig. 3). More infiltrating cells were observed in the abdominal lavage fluid of M1- and M2-treated mice than M3- and S4-treated mice, the latter having similar numbers as the control. In particular, M1, which is longer than M2, showed a significant increase in the number of infiltrating cells and induced inflammatory cell accumulation. These results indicated that large MWCNTs cause potent inflammation and DNA damage *in vitro* and *in vivo*.

Interestingly, significant differences in the inflammatory effects were observed between CNTs of different size and shape. However, the reason for this difference is not clear. Recently, silica particles or asbestos have been reported to activate the inflammasome and cause IL-1β production and *in vivo* inflammation [18, 19]. Based on these findings, although further examination is necessary, we hypothesize that CNTs may also elicit inflammasome formation similar to that observed by silica and asbestos treatment.

In general, it is known that inflammation can increase cancer risk and can promote tumor progression at various stages of tumorigenesis [20, 21]. Inflammation may contribute to tumor initiation by inducing DNA damage through intermediates like reactive oxygen species [21]. During tumor promotion, inflammatory cells produce cytokines and chemokines, which facilitate cancer cell survival, proliferation, and promote the angiogenic switch, resulting in increased tumor growth [20]. In this study, we did not examine the linkage between DNA damage and inflammation induced by carbon nanotubes. But we consider that DNA damage and inflammation induced by CNT might increase cancer risk of CNT.

In summary, unlike SWCNT, MWCNTs cause DNA damage and inflammation, the extent of which is related to the length and thickness of the CNTs. These effects are related to an increased risk of carcinogenic activity due to DNA damage and inflammatory effect. In addition, these results indicate that short and thin MWCNT do not cause DNA damage and inflammation, indicating that these MWCNT may be useful MWCNT with safety. We believe that the knowledge obtained by these studies might provide both useful information for updating existing regulatory systems and guidelines that are suitable for ensuring the safety of CNTs.

ACKNOWLEDGMENTS

This study was supported in part by Grants-in-Aid for Scientific Research from the Ministry of Education, Culture, Sports, Science, and Technology of Japan, and

from the Japan Society for the Promotion of Science (JSPS). This study was also supported in part by Health Labor Sciences Research Grants from the Ministry of Health, Labor, and Welfare of Japan; by Health Sciences Research Grants for Research on Health Sciences focusing on Drug Innovation from the Japan Health Sciences Foundation; by a Grant from the Minister of the Environment; and by The Nagai Foundation Tokyo.

REFERENCES

1. Sternand, S.T., and S.E. McNeil. 2008. Nanotechnology safety concerns revisited. *Toxicol Sci* 101: 4–21.
2. Lacerda, L., A. Bianco, M. Prato, and K. Kostarelos. 2006. Carbon nanotubes as nanomedicines: From toxicology to pharmacology. *Adv Drug Deliv Rev* 58: 1460–1470.
3. Tran, P., L. Zhang, and T.J. Webster. 2009. Carbon nanofibers and carbon nanotubes in regenerative medicine. *Adv Drug Deliv Rev* 61: 1097–1114.
4. Donaldson, K., R. Aitken, L. Tran, V. Stone, R. Duffin, G. Forrest, and A. Alexander. 2006. Carbon nanotubes: A review of their properties in relation to pulmonary toxicology and workplace safety. *Toxicol Sci* 92: 5–22.
5. Maynard, A.D. 2007. Nanotechnology: The next big thing, or much ado about nothing? *Ann Occup Hyg* 51: 1–12.
6. Kaneand, A.B., and R.H. Hurt. 2008. Nanotoxicology: The asbestos analogy revisited. *Nat Nanotechnol* 3: 378–379.
7. Shvedova, A.A., E.R. Kisin, D. Porter, P. Schulte, V.E. Kagan, B. Fadeel, and V. Castranova. 2009. Mechanisms of pulmonary toxicity and medical applications of carbon nanotubes: Two faces of Janus? *Pharmacol Ther* 121: 192–204.
8. Poland, C.A., R. Duffin, I. Kinloch, A. Maynard, W.A. Wallace, A. Seaton, V. Stone, S. Brown, W. Macnee, and K. Donaldson. 2008. Carbon nanotubes introduced into the abdominal cavity of mice show asbestos-like pathogenicity in a pilot study. *Nat Nanotechnol* 3: 423–428.
9. Takagi, A., A. Hirose, T. Nishimura, N. Fukumori, A. Ogata, N. Ohashi, S. Kitajima, and J. Kanno. 2008. Induction of mesothelioma in p53+/- mouse by intraperitoneal application of multi-wall carbon nanotube. *J Toxicol Sci* 33: 105–116.
10. Sakamoto, Y., D. Nakae, N. Fukumori, K. Tayama, A. Maekawa, K. Imai, A. Hirose, T. Nishimura, N. Ohashi, and A. Ogata. 2009. Induction of mesothelioma by a single intrascrotal administration of multi-wall carbon nanotube in intact male Fischer 344 rats. *J Toxicol Sci* 34: 65–76.
11. Shibata, H., Y. Yoshioka, A. Ohkawa, K. Minowa, Y. Mukai, Y. Abe, M. Taniai, T. Nomura, H. Kayamuro, H. Nabeshi, T. Sugita, S. Imai, K. Nagano, T. Yoshikawa, T. Fujita, S. Nakagawa, A. Yamamoto, T. Ohta, T. Hayakawa, T. Mayumi, P. Vandenabeele, B. B. Aggarwal, T. Nakamura, Y. Yamagata, S. Tsunoda, H. Kamada, and Y. Tsutsumi. 2008. Creation and X-ray structure analysis of the tumor necrosis factor receptor-1-selective mutant of a tumor necrosis factor-alpha antagonist. *J Biol Chem* 283: 998–1007.
12. Maynard, S., S.H. Schurman, C. Harboe, N.C. de Souza-Pinto, and V.A. Bohr. 2009. Base excision repair of oxidative DNA damage and association with cancer and aging. *Carcinogenesis* 30: 2–10.
13. Mossmanand, B.T., and A. Churg. 1998. Mechanisms in the pathogenesis of asbestosis and silicosis. *Am J Respir Crit Care Med* 157: 1666–1680.
14. Kampand, D.W., and S.A. Weitzman. 1999. The molecular basis of asbestos induced lung injury. *Thorax* 54: 638–652.
15. Pollard, J.W. 2004. Tumour-educated macrophages promote tumour progression and metastasis. *Nat Rev Cancer* 4: 71–78.
16. Clevers, H. 2004. At the crossroads of inflammation and cancer. *Cell* 118: 671–674.
17. Krelin, Y., E. Voronov, S. Dotan, M. Elkabets, E. Reich, M. Fogel, M. Huszar, Y. Iwakura, S. Segal, C.A. Dinarello, and R.N. Apte. 2007. Interleukin-1beta-driven inflammation promotes the development and invasiveness of chemical carcinogen-induced tumors. *Cancer Res* 67: 1062–1071.
18. Dostert, C., V. Petrilli, R. Van Bruggen, C. Steele, B.T. Mossman, and J. Tschopp. 2008. Innate immune activation through Nalp3 inflammasome sensing of asbestos and silica. *Science* 320: 674–677.
19. Cassel, S.L., S.C. Eisenbarth, S.S. Iyer, J.J. Sadler, O.R. Colegio, L.A. Tephly, A.B. Carter, P.B. Rothman, R.A. Flavell, and F.S. Sutterwala. 2008. The Nalp3 inflammasome is essential for the development of silicosis. *Proc Natl Acad Sci U S A* 105: 9035–9040.
20. Mantovani, A., P. Allavena, A. Sica, and F. Balkwill. 2008. Cancer-related inflammation. *Nature* 454: 436–444.
21. Grivennikov, S.I., and M. Karin. 2009. Inflammation and oncogenesis: a vicious connection. *Curr Opin Genet Dev.* doi:10.1016/j.gde.2009.11.004.

Biomaterials 31 (2010) 6833–6842

Contents lists available at ScienceDirect

Biomaterials

journal homepage: www.elsevier.com/locate/biomaterials

The effect of surface modification of amorphous silica particles on NLRP3 inflammasome mediated IL-1β production, ROS production and endosomal rupture

Tomohiro Morishige [a,1], Yasuo Yoshioka [a,b,c,*,1], Hiroshi Inakura [a], Aya Tanabe [a], Xinglei Yao [a], Shogo Narimatsu [a], Youko Monobe [d], Takayoshi Imazawa [d], Shin-ichi Tsunoda [b,c], Yasuo Tsutsumi [b,c,e], Yohei Mukai [a], Naoki Okada [a], Shinsaku Nakagawa [a,b,**]

[a] Laboratory of Biotechnology and Therapeutics, Graduate School of Pharmaceutical Sciences, Osaka University, 1–6 Yamadaoka, Suita, Osaka 565–0871, Japan
[b] The Center for Advanced Medical Engineering and Informatics, Osaka University, 1–6 Yamadaoka, Suita, Osaka 565–0871, Japan
[c] Laboratory of Pharmaceutical Proteomics, National Institute of Biomedical Innovation, 7–6–8 Saito-Asagi, Ibaraki, Osaka 567–0085, Japan
[d] Laboratory of Common Apparatus, Division of Biomedical Research, National Institute of Biomedical Innovation, 7–6–8 Saito-Asagi, Ibaraki, Osaka 567–0085, Japan
[e] Laboratory of Toxicology and Safety Science, Graduate School of Pharmaceutical Sciences, Osaka University, 1–6 Yamadaoka, Suita, Osaka 565–0871, Japan

ARTICLE INFO

Article history:
Received 23 April 2010
Accepted 18 May 2010
Available online 18 June 2010

Keywords:
Cytokine
Inflammation
Interleukin
Macrophage
Nanoparticle
Silica

ABSTRACT

Although amorphous silica particles (SPs) are widely used in cosmetics, foods and medicinal products, it has gradually become evident that SPs can induce substantial inflammation accompanied by interleukin-1β (IL-1β) production. Here, to develop safe forms of SPs, we examined the mechanisms of SP-induced inflammation and the relationship between particle characteristics and biological responses. We compared IL-1β production levels in THP-1 human macrophage like cells in response to unmodified SP of various diameters (30- to 1000-nm) and demonstrated that unmodified microsized 1000-nm SP (mSP1000) induced higher levels of IL-1β production than did smaller unmodified SPs. Furthermore, we found that unmodified mSP1000–induced IL-1β production was depended on the sequence of reactive oxygen species (ROS) production, endosomal rupture, and subsequent activation of pro-inflammatory complex NLRP3 inflammasome. In addition, we compared IL-1β production levels in THP-1 cells treated with mSP1000s modified with a functional group (−COOH, $-NH_2$, $-SO_3H$, −CHO). Although unmodified and surface-modified mSP1000s were taken up with similar frequencies equally into the THP-1 cells, surface modification of mSP1000 dramatically suppressed IL-1β production by reducing ROS production. Our results reveal a part of NLRP3 activation pathway and provide basic information that should help to create safe and effective forms of SPs.

1. Introduction

Amorphous (noncrystalline) silica particles (SPs) possess extraordinary advantages, including straightforward synthesis, relatively low cost, easy separation, and easy surface modification. In addition, SPs are usually considered to have low toxicity, in contrast to crystalline silica, which can cause silicosis and some forms of lung cancer [1,2]. Therefore, SPs have been used for many applications, including in cosmetics, foods, medical diagnosis, cancer therapy, and drug delivery [3–7].

However, the increasing use of SPs has raised public concern about their safety. In fact, current studies have found that SPs induce substantial lung inflammation accompanied by the expression of inflammatory cytokines, including interleukin-1β (IL-1β) [8–10]. Inflammation has been suggested as the key factor in the development of chronic obstructive pulmonary disease (COPD), fibrosis, and carcinogenesis [11–13]. There is therefore an urgent need to investigate the biological inflammatory effects of SPs and ensure their safe use. In addition, it has recently become evident that particle characteristics, including particle size and surface properties, are important factors in pathologic alterations and cellular responses [14–16]. Therefore, for the further development

* Corresponding author at: The Center for Advanced Medical Engineering and Informatics, Osaka University, 1-6 Yamadaoka, Suita, Osaka 565-0871, Japan. Tel./fax: +81 6 6879 8177.
** Corresponding author at: Laboratory of Biotechnology and Therapeutics, Graduate School of Pharmaceutical Sciences, Osaka University, 1-6 Yamadaoka, Suita, Osaka 565-0871, Japan. Tel.: +81 6 6879 8175; fax: +81 6 6879 8179.
E-mail addresses: yasuo@phs.osaka-u.ac.jp (Y. Yoshioka), nakagawa@phs.osaka-u.ac.jp (S. Nakagawa).
[1] Each author contributed equally to the work.

0142-9612/$ – see front matter © 2010 Elsevier Ltd. All rights reserved.
doi:10.1016/j.biomaterials.2010.05.036

of safe SPs, investigation of the mechanisms of SP-induced inflammation and development of a methodology to decrease their inflammatory effects on the basis of evidence of the correlation between particle characteristics and biological effects are very important.

IL-1β is involved in initiation of the inflammatory process and thus contributes to acute and chronic inflammatory diseases. In fact, Cassel et al. reported the possibility that IL-1β induced by inhalation of crystalline silica and asbestos is essential for the development of silicosis and asbestosis, and thus it is needed to investigate whether SPs induce IL-1β production [17–19]. Among the most important sources of IL-1β against inhaled foreign particles are macrophages, which are widely known as the first line of defense [20]. Recently, several studies have shown that the action of macrophage-derived IL-1β is mediated by the activation of a multi-protein complex, called nucleotide-binding oligomerization domain–leucine-rich repeats containing pyrin domain 3 (NLRP3) inflammasome [20]. Production of the cytoplasmic NLRP3 is associated with fever syndromes characterized by spontaneous inflammation [21]. After being activated, NLRP3 interacts with the adaptor molecule apoptosis-associated speck-like protein containing a caspase recruitment domain (ASC) to form a pro-inflammatory complex, NLRP3 inflammasome, which is the principal caspase-1 activator [17,22,23]. Active caspase-1 catalyzes cleavage of the pro-cytokine IL-1β, which is secreted and biologically active only in processed form [23]. Thus, NLRP3 inflammasome is now gaining attention for its role in the initial inflammation generated in response to a number of diverse stimuli [22,24–26]. However, it is unclear whether SPs induce NLRP3 inflammasome activation. Moreover, the mechanisms of activation of NLRP3 inflammasome are poorly understood.

With the aim of developing safe forms of SPs, we evaluated the correlation between inflammatory effect and particle characteristics of SPs of various sizes or with various surface modification groups. Furthermore, we investigated the mechanisms of IL-1β production induced by SPs, concentrating on NLRP3 inflammasome.

2. Materials and methods

2.1. Materials and reagents

Unmodified SPs of diameters between 30 and 1000 nm [nanosized (n)SP30, nSP70, and nSP300, and microsized (m)SP1000], various surface-modified 1000-nm SPs (mSP1000–COOH, $-NH_2$, $-SO_3H$, and –CHO) and FITC-conjugated mSP1000s (unmodified, –COOH, $-NH_2$, $-SO_3H$, and –CHO) were purchased from Micromod Partikeltechnologie (Rostock/Warnemünde, Germany). Phorbol 12-myristate 13-acetate (PMA), cytochalasin D, butylated hydroxyanisole (BHA), and diphenyleneiodonium chloride (DPI) were purchased from Sigma–Aldrich (St. Louis, MO). Bafilomycin A_1 was purchased from Biomol (Plymouth Meeting, PA). CA-074-methyl ester (CA-074-Me), zVAD-fmk, and zYVAD-fmk was purchased from Merck (Darmstadt, Germany).

2.2. Cells and mice

THP-1 (human acute monocytic leukemia cell line) cells were obtained from the American Type Culture Collection (Manassas, VA) and cultured at 37 °C in RPMI (Wako Pure Chemical Industries, Osaka, Japan) supplemented with 10% FBS, 2 mM L-glutamine, and antibiotics. Female C57BL/6 mice were purchased from Nippon SLC (Shizuoka, Japan) and used at 8 weeks of age. All of the animal experimental procedures were performed in accordance with Osaka University's guidelines for the welfare of animals.

2.3. Characterization of silica particle

Size distribution of each SP was measured using a Zetasizer 3000HS (Worcestershire, UK) after sonication with a particle concentration of 300 μg/mL in H_2O.

2.4. Cytotoxicity assay and enzyme-linked immunosorbent assay (ELISA)

THP-1 cells (1.5×10^4 cells/well) were seeded in 96-well plates (Nunc, Rochester, NY) and were then differentiated into macrophages by incubation with 0.5 μM PMA at 37 °C for 24 h followed by one wash with cell culture medium. After the PMA priming, cells were treated with SPs at 100 μg/mL or 3 mM ATP for 6 or 24 h. Cytotoxicity of the SPs was assessed by the standard methylene blue assay method, as previously described [27]. IL-1β production levels in the culture supernatants were assessed with an ELISA kit (BD Pharmingen, San Diego, CA) in accordance with the manufacturer's instructions. For the inhibitory assay, PMA-primed THP-1 cells were pre-incubated for 30 min with cytochalasin D (5 μM), zYVAD-fmk (10 μM), CA-074-Me (2 μM), bafilomycin A_1 (250 nM), BHA (150 μM), DPI (60 μM), or zVAD-fmk (60 μM). The cells were then treated with SPs at 100 μg/mL or with 3 mM ATP for 6 or 24 h.

2.5. In vivo inflammatory effect

C57BL/6 mice were intraperitoneally injected with 1 mg mSP1000s in 200 μL PBS. Six hours after the treatment, the mice were sacrificed and all of the peritoneal cavity lavage fluid (PCLF) was collected in 4 mL PBS. The total number of live cells in the PCLF was determined with a NucleoCounter (Chemometec A/S, Allerød, Denmark).

2.6. Laser scanning confocal microscopy analysis

THP-1 cells (1×10^5 cells/well) were primed with PMA on a Lab-Tek II Chambered Coverglass (Nunc) and incubated for 6 h with 500 μg/mL 10-kDa dextran conjugated with Alexa Fluor 594 (Invitrogen, Carlsbad, CA) and 100 μg/mL mSP1000. The cells were washed and then fixed with 4% paraformaldehyde, and mounted with Prolong Gold Antifade Reagent with DAPI (Invitrogen) for nuclear staining. Fluorescence was observed under a laser scanning confocal microscope (TCS SP2 AOBS; Leica Microsystems, Wetzlar, Germany).

2.7. Transmission electron microscopy (TEM) analysis

THP-1 cells (1×10^5 cells/well) were primed with PMA on a Lab-Tek II Chambered Coverglass and incubated for 6 h with 100 μg/mL mSP1000. They were then fixed in 2.5% glutaraldehyde followed by 1.5% osmium tetraoxide. The fixed cells were dehydrated and embedded in EPON resin. Ultrathin sections were stained with lead citrate and observed by TEM.

2.8. Flow cytometry

THP-1 cells (7×10^5 cells/well) were primed with PMA on 6-well plates and treated with 100 μg/mL mSP1000s for 6 h at 37 °C or 4 °C. After the treatment, cells were detached from the tissue culture plates by incubation with trypsin. Cells were then washed and evaluated in accordance with the Fluorescence-1 (FL-1) parameter using a FACSCalibur flow cytometer (Becton Dickinson, Franklin Lakes, NJ) and Flow Jo software (Three Star, Ashland, OR). Cells were gated to exclude SPs and small cell debris (low forward scatter). Cells with increased FL-1 fluorescence were expressed as a percentage of the maximum number (50,000) of gated cells.

2.9. Reverse transcription polymerase chain reaction (RT-PCR)

THP-1 cells (7×10^5 cells/well) were primed with PMA on 6-well plates and treated with 100 μg/mL mSP1000s for 3 h. After the treatment, total RNA was extracted from the cells by using Sepasol RNA-1 Super (Nacalai Tesque, Kyoto, Japan) in accordance with the manufacturer's instructions. Extracted RNA was reverse-transcribed with SuperScript III (Invitrogen). Synthesized cDNA was amplified by PCR using *Taq* DNA polymerase (Toyobo, Osaka, Japan). The sequences of the specific primers for IL-1β and GAPDH were as follows: IL-1β (F), 5′-AGAAGAACCTATCTTCTTCGA-3′; IL-1β (R), 5′-ACTCTCCAGCTGTAGAGTG G-3′; GAPDH (F), 5′-GCAGGGGGGAGCCAAAAGGG-3′; and GAPDH (R), 5′-TGCCAGCCCCAGCGTCAAAG-3′. After denaturation for 2 min at 95 °C, 20 cycles of three sequential steps—denaturation for 30 s at 95 °C, annealing for 30 s at 60 °C, and extension for 60 s at 72 °C—were performed, ending with a final extension step for 5 min at 72 °C. The PCR products were electrophoresed through a 2% agarose gel, stained with ethidium bromide, and visualized under ultraviolet radiation.

2.10. Observation of activated NLRP3 inflammasome

PMA-primed THP-1 cells were transiently transfected with the plasmid encoding cyan fluorescent protein (CFP)–ASC fusion protein (CFP–ASC) by using ExGen500 *in vitro* transfection agent (Fermentas, Baltimore, MD) in accordance with the manufacturer's instructions [25]. In brief, THP-1 cells (1×10^5 cells/well) were primed with PMA on Lab-Tek II Chambered Coverglass. The cells were then incubated for 60 h in 550 μL of cell culture medium containing the CFP–ASC plasmid (2 μg) – ExGen500 (50 μL) complex. The cells were washed and then treated with 100 μg/mL unmodified mSP1000 for 4 h. After the treatment, the cells were washed and then fixed with 4% paraformaldehyde. They were then mounted with Prolong

Gold Antifade Reagent (Invitrogen). Fluorescence was observed under a confocal laser scanning microscope.

2.11. Evaluation of reactive oxygen species (ROS) production

THP-1 cells (3×10^4 cells/well) were primed with PMA on 96-well black plates (Nunc) and treated with 100 μg/mL mSP1000s for 24 h. The cells were then incubated with 10 μM 2′,7′-dichlorodihydrofluorescein diacetate, acetyl ester (H_2DCFDA; Invitrogen) for 45 min and washed with PBS. Fluorescence was measured at $OD_{485-530}$ using a multi-well spectrophotometer (Molecular Devices, Inc., Tokyo, Japan). ROS production intensity was calculated by using the following formula: ROS production intensity = fluorescence/cell viability. The ROS production intensity of untreated control cells was arbitrarily set to 100%.

2.12. Statistical analysis

All results are presented as means ± SD or SEM. Differences were compared by using Student's *t*-test or Bonferroni's method after ANOVA.

3. Results

3.1. IL-1β production of SPs

To assess the correlation between particle size and the inflammatory effect of SPs, we examined the levels of IL-1β production induced by SPs in THP-1 macrophage-like cells (Fig. 1 A, B). First, we used unmodified SPs of five diameters between 30 and 1000 nm (unmodified nSP30, nSP50, nSP70, and nSP300, and unmodified mSP1000). The mean secondary particle diameters of each SP, measured by Zetasizer, were 33, 44, 79, 326, and 945 nm, respectively (data not shown). We already confirmed that these silica particles were smooth-surfaced spheres and well-dispersing by transmission electron microscopy (data not shown). We incubated THP-1 cells with SPs of each size for 6 h and then analyzed the levels of IL-1β in the culture supernatant. Unmodified mSP1000 induced significantly higher IL-1β production than PBS control, whereas the other, smaller SPs did not induce IL-1β production (Fig. 1A).

Next, to assess the correlation between surface modification and the inflammatory effect of SPs, we used mSP1000s with various surface-modification groups (unmodified, or with an added -COOH, $-NH_2$, $-SO_3H$, or -CHO group) (Fig. 1B). The mean secondary particle diameters of each type of mSP1000 were 945, 1022, 958, 1023, and 969 nm, respectively (data not shown). We incubated THP-1 cells with these surface-modified particles for 6 or 24 h and then examined the IL-1β production levels. Unmodified mSP1000 induced significantly greater IL-1β production than did the medium controls at both 6 and 24 h, whereas the surface-modified mSP1000s induced low levels of IL-1β production (Fig. 1B). The rank order of IL-1β production levels was unmodified mSP1000 > $-$COOH > $-NH_2 = -SO_3H = -$CHO. Furthermore, we evaluated the inflammatory effect of each type of mSP1000 *in vivo*. We intraperitoneally injected mSP1000s into C57CL/6 mice and analyzed the total number of live cells in the PCLF, because inflammation induces local infiltration by various inflammatory cells (Fig. 1C) [28]. The unmodified mSP1000 induced significantly greater cell migration than did the PBS control. The surface-modified mSP1000s did not induce cell accumulation beyond the control level. The rank order of the *in vivo* inflammatory effect was tended to the same as that of IL-1β production *in vitro*. These results indicate that appropriate surface modification with a functional group suppresses the inflammatory effect of unmodified mSP1000.

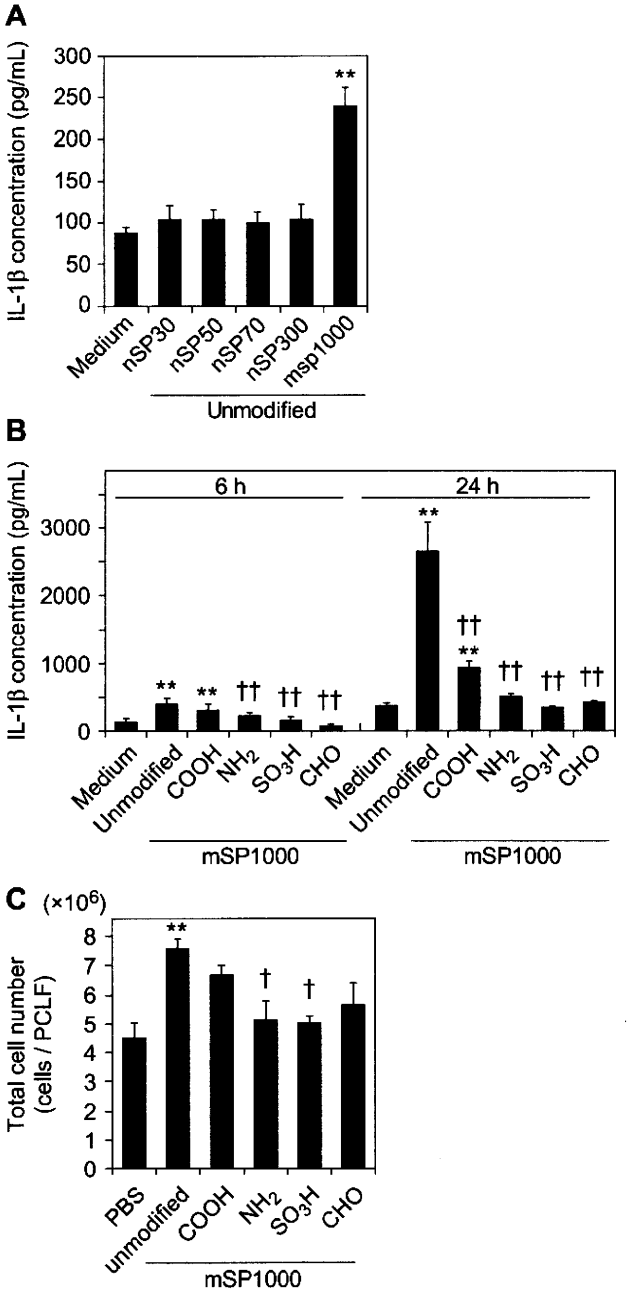

Fig. 1. Correlation between SP characteristics and inflammatory effects *in vitro* and *in vivo*. (A, B) IL-1β production levels in response to SPs of various sizes or with various surface modifications. PMA-primed THP-1 cells were treated with (A) unmodified SPs (30 nm–1000 nm) or (B) unmodified mSP1000, or mSP1000s modified with -COOH, $-NH_2$, $-SO_3H$, or -CHO for 6 or 24 h. IL-1β production levels in the culture supernatant were measured by ELISA. Data represent means ± SD ($n = 5$; $^{**}P < 0.01$ versus value for medium control, $^{\dagger\dagger}P < 0.01$ versus value for unmodified mSP1000, ANOVA). (C) Inflammatory effects of mSP1000s *in vivo*. Mice were intraperitoneally injected with PBS or with 1 mg of one type of mSP1000, and the total numbers of live cells in the PCLF were evaluated after 6 h. Data represent means ± SEM ($n = 5$; $^{*}P < 0.05$ versus value for PBS control, $^{\dagger}P < 0.05$ versus value for unmodified mSP1000, ANOVA).

3.2. Phagocytosis of mSP1000s

Through their phagocytic activity, macrophages play an important role in determining the bio-persistence of foreign particles and initiating inflammatory responses, including IL-1β production [29]. Therefore, to investigate whether mSP1000-induced IL-1β production was triggered by phagocytosis, we pretreated THP-1 cells with cytochalasin D, a well-characterized inhibitor of phagocytosis that impairs actin filament assembly (Fig. 2A). We then

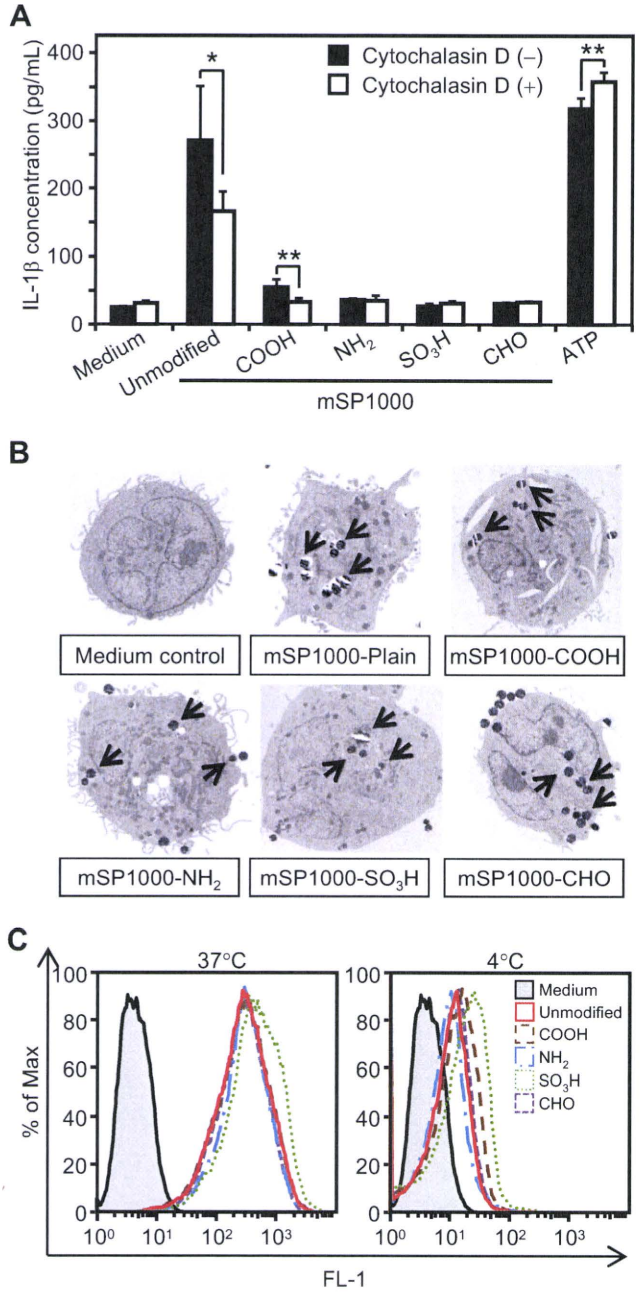

Fig. 2. Phagocytosis is a first signal for mSP1000-induced IL-1β production. (A) Involvement of phagocytosis in mSP1000-induced IL-1β production. PMA-primed THP-1 cells were treated with mSP1000s or ATP for 6 h in the absence (black bars) or presence (white bars) of cytochalasin D (5 μM). IL-1β production levels were then measured by ELISA. Data represent means ± SD ($n = 5$; $^{*}P < 0.05$, $^{**}P < 0.01$ versus value for cytochalasin D [−] control within each treatment pair, *t*-test). (B) TEM analysis of mSP1000s. PMA-primed THP-1 cells were treated with mSP1000s for 6 h. Cells were then observed by TEM. Arrows indicate ingested mSP1000s. (C) Flow cytometry of FITC-mSP1000s taken up into PMA-primed THP-1 cells. Cells were treated with mSP1000s and incubated for 6 h at 37 °C (left) or 4 °C (right). Data were analyzed by using the FL-1 parameter for green fluorescence.

treated the cells with mSP1000s or ATP, a well-known caspase-1 activator without cellular internalization. The cytochalasin D abolished the mSP1000-induced IL-1β production, whereas the response to ATP was unaffected (Fig. 2A). These results indicate that cellular ingestion of mSP1000s might be the first signal in the inflammatory response. We then speculated that the reduction in IL-1β production through surface modification of mSP1000s resulted from a change in the particle uptake frequency. We used TEM and flow cytometry to evaluate the frequency of uptake of mSP1000s (Fig. 2B, C). TEM analysis clearly showed that both the modified and unmodified mSP1000s were taken up by THP-1 cells (Fig. 2B). Furthermore, flow-cytometric analysis using FITC-conjugated mSP1000s showed that the frequencies of cellular ingestion of modified and unmodified mSP1000s were comparable at 37 °C (Fig. 2C). We also noted that the intensity of FITC-derived fluorescence was almost the same among the different types of mSP1000, and that the increase in the FL-1 signals was dose dependent (data not shown). These results collectively indicate that the unmodified and surface-modified mSP1000s were taken up with similar frequencies equally into the THP-1 cells by actin-dependent phagocytosis, independent of the type of modification group. Therefore, we considered that the difference in IL-1β production levels among mSP1000s was resulted from the signaling intensity in the IL-1β production cascade after ingestion of the mSP1000s by the cell.

3.3. Activation of caspase-1 by mSP1000s

IL-1β production is regulated by pro-IL-1β mRNA expression levels and by caspase-1 activity [17,22,23]. Therefore, to examine the mechanisms of the reduction in IL-1β production by surface modification, we used semi-quantitative RT-PCR to investigate the expression levels of pro-IL-1β mRNA in THP-1 cells treated with each type of mSP1000 (Fig. 3A). There were no significant differences in the expression levels of pro-IL-1β mRNA between cells treated with unmodified and modified mSP1000s. We then tested whether the reduction in IL-1β production by surface modification of mSP1000s resulted from changes in caspase-1 activity induced by mSP1000s. To investigate the association of caspase-1 activity with mSP1000-induced IL-1β production, we treated cells with mSP1000s in the presence of a caspase-1 specific inhibitor, zYVAD-fmk, and analyzed the IL-1β production levels (Fig. 3B). The results showed that zYVAD-fmk almost completely abrogated the IL-1β production induced by mSP1000s. These results collectively indicate that the IL-1β production induced by unmodified mSP1000 depend on the activation of caspase-1. Furthermore, it was speculated that the surface-modified mSP1000s induced little caspase-1 activation.

3.4. Activation of NLRP3 inflammasome by unmodified mSP1000

Recently, NLRP3 inflammasome was identified as the principal activator of caspase-1 in response to several types of danger signal [17,22,23]. To examine whether unmodified mSP1000 exerts their inflammatory potential through NLRP3 inflammasome, we examined the activation of NLRP3 inflammasome on THP-1 cells after treatment with unmodified mSP1000 (Fig. 4) [13,23]. We transiently transfected THP-1 cells with a plasmid expressing CFP–ASC fusion protein. ASC forms large oligomers after its activation, and the clustering of CFP–ASC can be used as an "optical reporter" of the activation of NLRP3 inflammasome [25,30]. Under baseline conditions CFP–ASC fluorescence was evenly distributed in the cytoplasm. Four hours after treatment with unmodified mSP1000, we detected bright fluorescent clusters of CFP–ASC in the cytoplasm. These clusters were not detected in non-transfected THP-1 cells treated with unmodified mSP1000, indicating that the clusters represented cytoplasmic aggregates of activated ASC in NLRP3 inflammasome. These results indicate that mSP1000-induced IL-1β production is mediated by the activation of NLRP3 inflammasome.

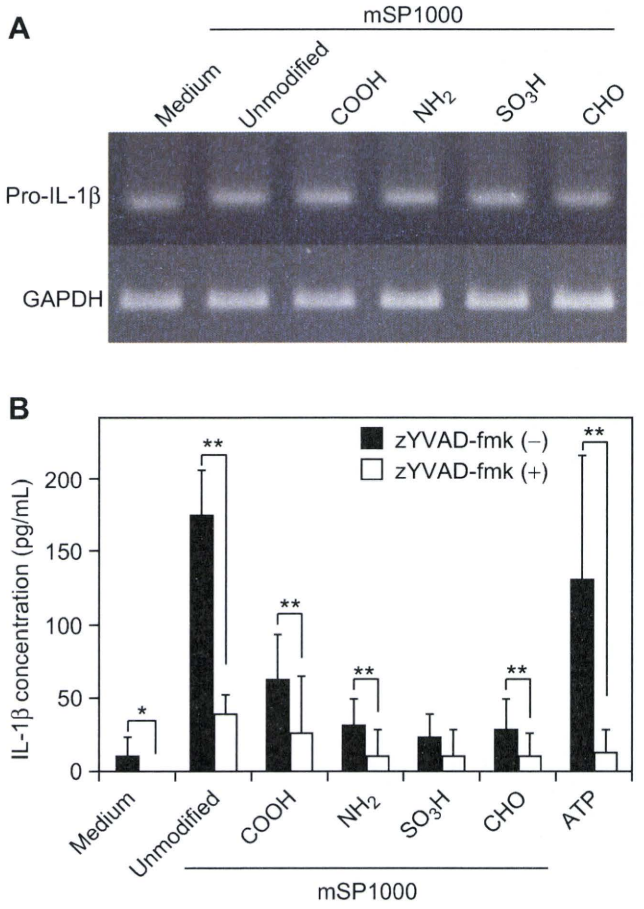

Fig. 3. Differences in levels of IL-1β production induced by each type of mSP1000 depend on caspase-1 activation. (A) Pro-IL-1β mRNA expression levels in mSP1000-treated cells. PMA-primed THP-1 cells were treated with mSP1000s and incubated for 3 h. Then, total RNA was isolated, and RT-PCR was performed with primers specific for IL-1β (top) or GAPDH (bottom). (B) Involvement of caspase-1 activity in mSP1000-induced IL-1β production. PMA-primed THP-1 cells were treated with each type of mSP1000 or with ATP for 6 h in the absence (black bars) or presence (white bars) of zYVAD-fmk (10 μM). IL-1β production levels were analyzed by ELISA. Data represent means ± SD ($n = 5$; $^{*}P < 0.05$, $^{**}P < 0.01$ versus value for zYVAD-fmk [−] control within each treatment pair, *t*-test).

3.5. Endosomal rupture and cathepsin B leakage

With crystalline silica, Hornung et al. reported that endosomal rupture plays a central role in activation of NLRP3 inflammasome followed by leakage of cathepsin B, a endosomal hydrolytic enzyme [20]. To investigate the mechanisms of IL-1β production induced by mSP1000, we compared the frequency of endosomal rupture and subsequent cathepsin B leakage among each type of mSP1000, using Alexa Fluor 594 dextran as an endocytic compartment marker [31]. Mature endosomes incorporating dextran are observed as dotted forms, and the spread of dextran into the cytoplasm is recognized as an indicator of endosomal rupture [20]. We incubated THP-1 cells with dextran and different types of mSP1000 and observed the behavior of the ingested dextran by confocal microscopy (Fig. 5A). Upon treatment of the cells with unmodified mSP1000, we detected the obvious spread of dextran throughout the cytosol, unlike in untreated control cells, indicating that unmodified mSP1000 induced endosomal rupture (Fig. 5A). In contrast, the degree of endosomal rupture was decreased in cells treated with surface-modified mSP1000s, while mSP1000–COOH induced endosomal rupture to some extent as the IL-1β production levels (Fig. 5A). To investigate whether cathepsin B was involved in mSP1000-induced IL-1β production, we treated cells with mSP1000s in the presence of a specific inhibitor of vacuolar H^+-ATPase (bafilomycin A_1), which is needed to activate cathepsin B and a membrane-permeable cathepsin B-specific chemical inhibitor (CA-074-Me). Both inhibitors almost completely suppressed IL-1β production induced by mSP1000s (Fig. 5B and C). These results collectively suggest that the activation of NLRP3 inflammasome and subsequent IL-1β production induced by mSP1000s are triggered by active cathepsin B leakage into the cytoplasm. Furthermore, they suggest that the reduction in IL-1β production by surface modification of mSP1000s results from a reduction in the frequency of mSP1000-induced endosomal rupture and subsequent cathepsin B leakage.

3.6. ROS production of mSP1000s

Another study has shown that ROS, in addition to cathepsin B, plays a crucial role in NLRP3 activation [13,19]. To investigate whether mSP1000-induced activation of NLRP3 inflammasome is dependent on ROS, we measured the levels of ROS in mSP1000-treated THP-1 cells by H_2DCFDA [32]. Treatment of THP-1 cells with unmodified mSP1000, but not with surface-modified SP1000s, significantly enhanced ROS production compared with that in the medium control (Fig. 6A). To confirm the involvement of ROS in mSP1000-induced IL-1β production, we evaluated the levels of IL-1β induced by mSP1000s in the presence of a broad ROS scavenger, BHA, or a specific inhibitor of NADPH oxidase, DPI. NADPH oxidase is an important enzymatic source for the production of ROS [33]. We confirmed that both BHA and DPI significantly suppressed unmodified mSP1000–induced IL-1β production (Fig. 6B and C). These results indicate that, in addition to cathepsin B, mSP1000-induced ROS play an important role in NLRP3 activation.

We then examined the association between mSP1000-induced ROS production and endosomal rupture. We incubated cells with dextran and unmodified mSP1000 in the presence of BHA and observed the behavior of the dextran as a reflection of endosomal morphology. The endosomal rupture induced by unmodified mSP1000 was almost completely suppressed by BHA (Fig. 6D). These observations collectively suggest that ROS production induced by phagocytosis of unmodified mSP1000 triggered endosomal rupture followed by the activation of NLRP3 inflammasome and subsequent IL-1β production. Furthermore, they also strongly indicate that the reduction in ROS production by surface modification attributes to the decrement of the IL-1β production seen with unmodified mSP1000.

3.7. Cell death by unmodified mSP1000

We reported previously that mSP1000-induced cell death is dependent in part on ROS but independent of caspase-1, -3, -4, and -7, and we also showed that surface modification of mSP1000 significantly suppresses particle cytotoxicity [34]. Here, we speculated that mSP1000-induced cell death was dependent on cathepsin B leakage or on IL-1β signaling triggered by ROS production. Therefore, to investigate the association of cathepsin B and IL-1β signaling with mSP1000-induced cell death, we treated THP-1 cells with unmodified mSP1000 in the presence or absence of CA-074-Me, bafilomycin A_1, or zYVAD-fmk. CA-074-Me and bafilomycin A_1, but not zYVAD-fmk, significantly suppressed the cytotoxicity of unmodified mSP1000 (Fig. 6E). These findings indicate that unmodified mSP1000–induced cell death depends in part on ROS and active cathepsin B but is independent of caspases and IL-1β signals.

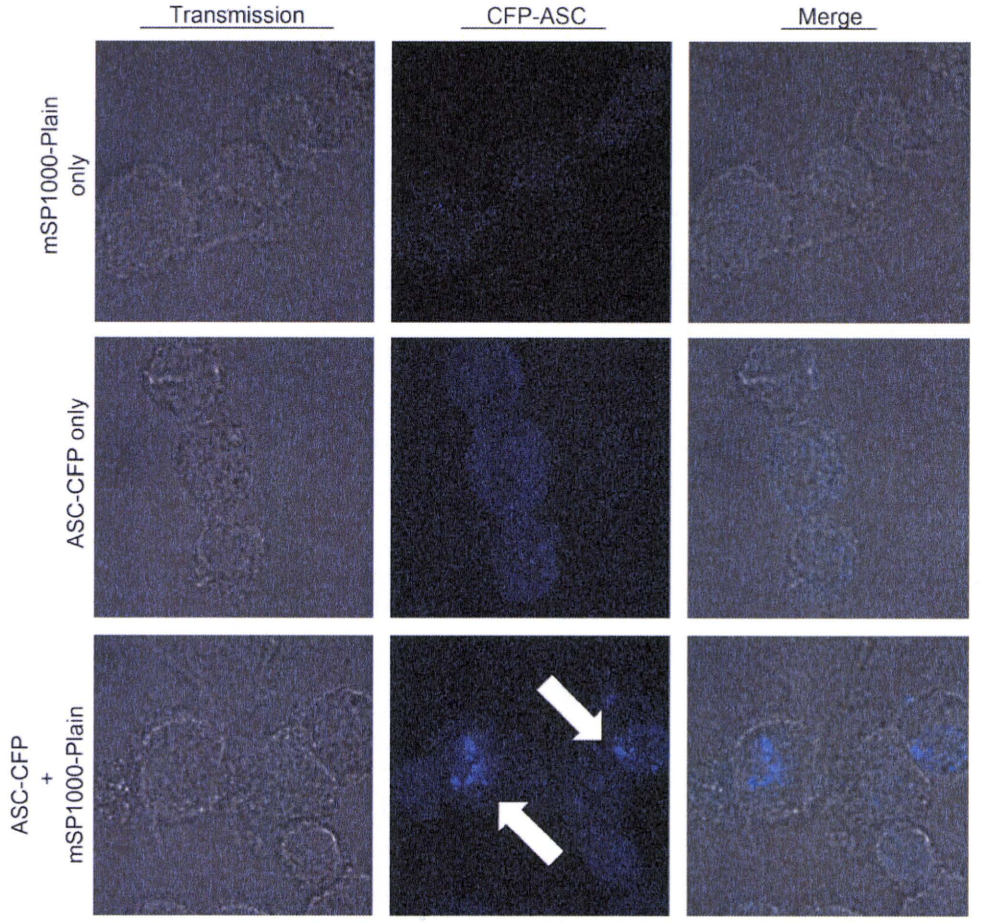

Fig. 4. Unmodified mSP1000–induced IL-1β production is mediated by activation of NALP3 inflammasome. PMA-primed THP-1 cells transiently transfected with CFP–ASC were treated with unmodified mSP1000. The cells were then observed by confocal microscopy. Treated with unmodified mSP1000 alone (top); untreated but transfected with CFP–ASC (middle); or treated with unmodified mSP1000 and transfected with CFP–ASC (bottom). Arrows indicate clusters of CFP–ASC (blue).

4. Discussion

Our goal was to elucidate the mechanisms of the inflammatory effects induced by SPs and to provide basic information for the creation of safe and effective SPs. To achieve these purposes, we focused on the IL-1β production induced by SPs, because IL-1β production is currently considered to play an important role in the initial inflammatory responses that lead to asbestosis and silicosis [19]. Our results provided evidence that unmodified mSP1000, but not smaller SPs, induces significant IL-1β production by THP-1 cells. Although the detailed mechanisms of this particle-size dependency in IL-1β production were unclear, we speculate that there are differences in the intracellular behavior of SPs and in the signaling pathways, and cytokine production patterns induced by SPs. Consistent with our hypothesis, our unpublished data showed that mSP1000s and the smaller SPs induce different inflammatory cytokine and chemokine production profiles (data not shown). Furthermore, many reports have shown that nanosized SPs induce inflammation *in vivo*. Therefore, we consider that it is also necessary to investigate the cytokine and chemokine production profiles induced by SPs of various sizes.

We then examined the effects of surface modification on mSP1000-induced IL-1β production, because it has become evident that surface properties are important factors in the biological effects of particles [14,15]. Interestingly, although unmodified and surface-modified mSP1000s were taken up equally, surface-modified mSP1000s induce little or no IL-1β production (Fig. 1B). The *in vivo* inflammatory effect was similarly reduced by surface modification of mSP1000s (Fig. 1C). We consider these results important to the creation of safe SPs.

Next, we examined the mechanisms of IL-1β production induced by mSP1000s to elucidate why surface modification reduced IL-1β production. First, we revealed that mSP1000-induced IL-1β production depends on the activation of NLRP3 inflammasome by using CFP–ASC fusion protein (Fig. 4). Some reports showed that other inflammasomes such as NLRP1 could activate caspase-1 in an ASC-dependent way [35]. Therefore we will need to confirm a specific role for NLRP3 in IL-1β production induced by mSP1000s by using siRNA of NLRP3 in future. A recent study showed that NLRP3 inflammasome mediated IL-1β production is associated with fever syndromes characterized by spontaneous inflammation [21]. In fact, the IL-1β receptor antagonist anakinra has been successfully used to treat patients suffering from inflammatory diseases, indicating that these patients have underlying increased IL-1β production [36,37]. However, the mechanisms of NLRP3 activation remain unclear, and therefore the definitive target to be overcome for the creation of safe materials is still unknown. Recently, different groups separately reported that cathepsin B leakage after endosomal rupture, as well as cytoplasmic ROS, plays a crucial role in the activation of NLRP3 inflammasome [13,20]. Consistent with these notions, we demonstrated here that mSP1000-induced IL-1β production is mediated by cathepsin B and

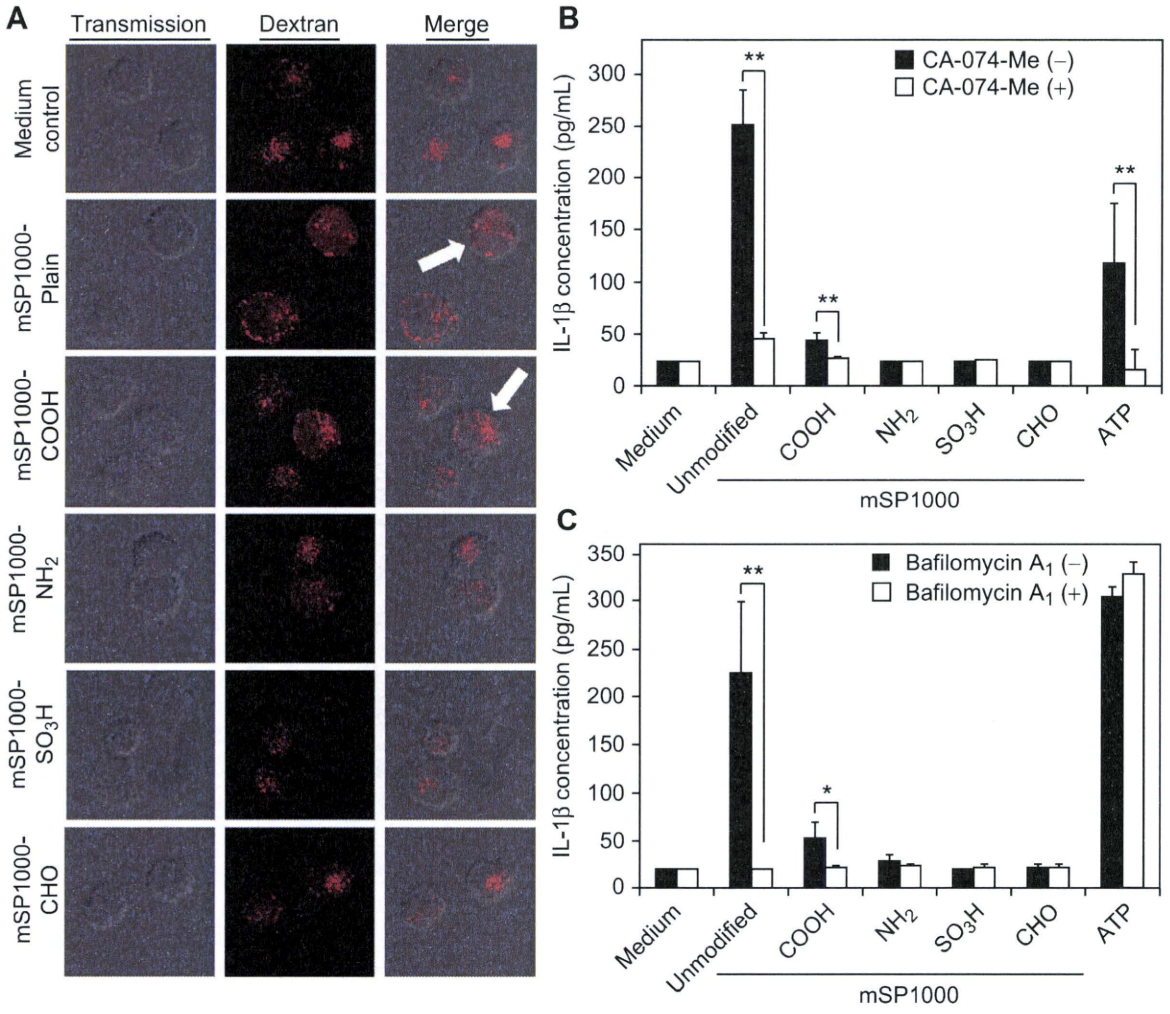

Fig. 5. mSP1000-induced IL-1β production is mediated by endosomal rupture. (A) Confocal microscopy of endosomal morphology. PMA-primed THP-1 cells were incubated with Alexa Fluor 594–conjugated dextran (red) and each type of mSP1000 for 6 h. The cells were then observed by confocal microscopy. Arrows show cells with spread of dextran into the cytoplasm, indicating endosomal rupture. (B, C) Involvement of cathepsin B in mSP1000-induced IL-1β production. PMA-primed THP-1 cells were treated with each type of mSP1000 or with ATP for 6 h in the absence (black bars) or presence (white bars) of (B) CA-074-Me (2 μM) or (C) bafilomycin A_1 (250 nM). Data represent means ± SD ($n = 5$; $^*P < 0.05$, $^{**}P < 0.01$ versus value for inhibitor [−] control within each treatment pair, *t*-test).

ROS (Figs. 5 and 6). However, it was unclear whether ROS and cathepsin B activate NLRP3 inflammasome separately or in a coordinated manner, and it was also unclear how endosomal rupture occurred. Use of a ROS inhibitor and surface-modified mSP1000s efficiently suppressed endosomal rupture (Fig. 6D). From these observations, we speculate that, with mSP1000 treatment, ROS trigger endosomal rupture and subsequent cathepsin B leakage into the cytosol, leading to the activation of NLRP3 inflammasome (Fig. 7). Our hypothesis is consistent with some reports suggesting that ROS trigger destabilization of the lysosomal membrane by membrane lipid oxidation [38].

In contrast, some reports have suggested that, in the case of crystalline silica, the reactive particle surface interacts with phagolysosomal membranes, leading to the release of endosomal enzymes into the cytosol after phagocytosis [39–41]. These contradictory findings suggest that various materials induce biological effects by different mechanisms in response to differences in particle characteristics. However, it remains unclear why the surface modification of mSP1000 reduced ROS production. It is possible that inappropriate surface modification induces an inflammatory effect stronger that of unmodified SP. We consider that further studies of the relationship between surface characteristics and bio-effect are necessary for the development of safe and effective materials. In this report, we found that DPI, an inhibitor of NADPH oxidase, significantly suppressed mSP1000-induced IL-1β production (Fig. 6C). NADPH oxidase is activated by the assembly of membrane lipids at local sites on the cellular surface and in the cytoplasm where the particles attach [42,43]. At this point, the silanol group (Si–OH) induces binding of the particles to membranes [44,45]. Therefore, we speculate that surface modification of mSP1000 masks the silanol group from the surface of the mSP1000 and blocks subsequent NADPH oxidase activation.

On the other hand, SP-induced cell death is also a critical obstacle, because macrophages play a central role in host defense systems. In 2007, Willingham et al. proposed a novel cell death pathway called pyronecrosis [46]. Induction of pyronecrosis is not dependent on IL-1β signaling or caspase-1 activity, although it requires the presence of the inflammasome component ASC and cathepsin B [46–48]. Our data suggested that mSP1000-induced cell death is independent of caspase-1 and IL-1β signaling but